Probing stratospheric transport and chemistry with new balloon and aircraft observations of the meridional and vertical N2O isotope distribution

J. Kaiser, A. Engel, R. Borchers, T. Röckmann

Atmos. Chem. Phys. Discuss., 6, 4273–4324, 2006
www.atmos-chem-phys-discuss.net/6/4273/2006/

Atmospheric Chemistry and Physics Discussions

Probing stratospheric transport and chemistry with new balloon and aircraft observations of the meridional and vertical N_2O isotope distribution

J. Kaiser[1,*], **A. Engel**[2], **R. Borchers**[3], **and T. Röckmann**[1,**]

[1]Atmospheric Physics Division, Max Planck Institute for Nuclear Physics, Heidelberg, Germany
[2]Institute for Atmosphere and Environment, J. W. Goethe University, Frankfurt, Germany
[3]Planets and Comets Department, Max Planck Institute for Solar System Research, Katlenburg-Lindau, Germany
[*]now at: School of Environmental Sciences, University of East Anglia, Norwich, UK
[**]now at: Institute for Marine and Atmospheric Research Utrecht, Utrecht University, The Netherlands

Received: 16 January 2006 – Accepted: 23 February 2006 – Published: 29 May 2006

Correspondence to: J. Kaiser (j.kaiser@uea.ac.uk)

Abstract

A comprehensive set of stratospheric balloon and aircraft samples was analyzed for the position-dependent isotopic composition of nitrous oxide (N_2O). Results for a total of 220 samples from between 1987 and 2003 are presented, nearly tripling the number of mass-spectrometric N_2O isotope measurements in the stratosphere published to date. Cryogenic balloon samples were obtained at polar (Kiruna/Sweden, 68° N), mid-latitude (southern France, 44° N) and tropical sites (Hyderabad/India, 18° N). Aircraft samples were collected with a newly-developed whole air sampler on board of the high-altitude aircraft M55 Geophysica during the EUPLEX 2003 campaign. All samples were analyzed by laboratory mass spectrometry for their $^{18}O/^{16}O$ and position-dependent $^{15}N/^{14}N$ isotope ratios with very high precision (standard deviation about 0.15‰ for $^{18}O/^{16}O$ and average $^{15}N/^{14}N$ ratios, about 0.5‰ for $^{15}NNO/^{14}NNO$ and $N^{15}NO/N^{14}NO$ ratios). For mixing ratios above 200 nmol mol^{-1}, relative isotope enrichments (δ values) and mixing ratios display a compact relationship, which is nearly independent of latitude and season and which can be explained equally well by Rayleigh fractionation or mixing. However, for mixing ratios below 200 nmol mol^{-1} this compact relationship gives way to meridional, seasonal and interannual variations. A comparison to a previously published mid-latitude balloon profile even shows large zonal variations, justifying the use of three-dimensional models for further data interpretation.

In general, the magnitude of the apparent fractionation constants (apparent isotope effects) increases continuously with altitude and decreases from the equator to the North pole, which can be qualitatively understood by the interplay between the time-scales of N_2O photochemistry and transport. Deviations from this behavior occur where polar vortex air mixes with nearly N_2O-free upper stratospheric/mesospheric air (e.g., during the boreal winter of 2003 and possibly 1992). Aircraft observations in the polar vortex at mixing ratios below 200 nmol mol^{-1} deviate from isotope variations expected for both Rayleigh fractionation and end-member mixing, but could be explained by continuous weak mixing between intravortex and extravortex air (Plumb et al., 2000).

Finally, correlations between $^{18}O/^{16}O$ and average $^{15}N/^{14}N$ isotope ratios or between the position-dependent $^{15}N/^{14}N$ isotope ratios show that photo-oxidation makes a large contribution to the total N_2O sink in the lower stratosphere (up to 100%). Towards higher altitudes, the temperature dependence of these isotope correlations becomes visible in the stratospheric observations.

1 Introduction

Stratospheric N_2O is enriched in the heavy nitrogen and oxygen isotopes (^{15}N, ^{17}O, ^{18}O) relative to tropospheric N_2O. This enrichment is caused by kinetic isotope fractionation in the stratospheric sink reactions, i.e., ultraviolet photolysis (R1) and reaction with electronically excited oxygen atoms, $O(^1D)$ (Reactions R2a+b):

$$N_2O + h\nu \rightarrow N_2 + O(^1D) \quad (185\,\text{nm} < \lambda < 225\,\text{nm}) \tag{R1}$$

$$N_2O + O(^1D) \rightarrow NO + NO \tag{R2a}$$

$$\rightarrow N_2 + O_2 \tag{R2b}$$

Reaction (R2) is also called "photo-oxidation", even though, strictly speaking, $O(^1D)$ only reacts as an oxidant in the NO+NO channel. Reaction (R1) accounts for about 90% of the total sink, whereas Reactions (R2a) and (R2b) contribute 6% and 4%, respectively (Minschwaner et al., 1993).

The dependence of the N_2O absorption spectrum on isotopic composition was already studied in the early 1980s (Selwyn and Johnston, 1981), but the relevance of this isotope effect for the ^{15}N enrichment observed in a single stratospheric N_2O sample (Moore, 1974) was not recognized before the early 1990s (Yoshida et al., 1990). Two additional stratospheric air samples analyzed by Kim and Craig (1993) substantiated the N_2O isotope enrichment for both ^{15}N and ^{18}O, but the results may have been impaired by CO_2 contamination (Rahn and Wahlen, 1997). Laboratory studies of isotope

fractionation in N_2O photolysis at 185 nm and during "photo-oxidation" found only small oxygen isotope effects (Johnston et al., 1995), in apparent contradiction to the stratospheric findings. However, additional high-quality field data from Rahn and Wahlen (1997) were accompanied by theoretical predictions of an increase of the photolytic isotope effect towards longer, stratospherically more relevant wavelengths (Yung and Miller, 1997). Laboratory measurements of isotope effects between 193 and 208 nm quickly showed that these theoretical predictions were qualitatively correct, but at least a factor of two too small in magnitude (Rahn et al., 1998). Analytical advances in the late 1990s then allowed the position-dependent measurement of the nitrogen isotope distribution between the terminal and central nitrogen atoms in N_2O (Brenninkmeijer and Röckmann, 1999; Esler et al., 2000; Toyoda and Yoshida, 1999). The new techniques were immediately adopted for extensive laboratory measurements of kinetic isotope effects during photolysis (summarized in Kaiser et al., 2003b; von Hessberg et al., 2004) and the reaction of N_2O with $O(^1D)$ (Kaiser et al., 2002a; Toyoda et al., 2004). Our present understanding of these isotope effects can be considered to be very good.

The new analytical techniques were used for further stratospheric measurements, as evidenced by six publications (Griffith et al., 2000; Park et al., 2004; Röckmann et al., 2001; Toyoda et al., 2001, 2004; Yoshida and Toyoda, 2000). The paper by Toyoda et al. (2004) also contains the data from the earlier two papers by the same principal authors. All but the Fourier transform infrared-spectra (FTIR) of Griffith et al. (2000) were analyzed by isotope ratio mass-spectrometry (IRMS) of discrete whole-air samples, either obtained by aircraft (Park et al., 2004) or from balloon platforms. A total of 32 samples were analyzed by Park et al. (2004). Toyoda and co-workers analyzed 72 samples. In the following, we present data from an additional 132 balloon and 88 aircraft samples, obtained at latitudes between 18° N and 80° N. A subset of ten tropical, one mid-latitude, and eight polar samples were already included in our previous paper (Röckmann et al., 2001). Importantly, we show two balloon profiles from Hyderabad/India at 18° N, the only existing stratospheric N_2O isotope measurements at

low latitudes. The tropics are important because there, the upwelling branches of the Hadley and the Brewer-Dobson circulation lead to net air mass transport from the troposphere to the stratosphere. Thus, the "youngest" stratospheric air masses are found in the tropics, where they undergo rapid photochemical processing. However, even though the geographic location of Hyderabad is in the tropics, this does not necessarily mean that the air mass sampled there can be considered tropical with respect to the atmospheric circulation system, as explained in Sect. 3.1. Further samples from the "deep" tropics might be needed to fully characterize the isotopic composition of N_2O in upwelling tropical air.

We will use tracer-tracer diagrams of stratospheric N_2O isotope and concentration measurements to investigate transport, mixing and photochemical processes (Sects. 3.2 and 3.3). Using correlations between isotope enrichments and mixing ratios, it will be shown to what extent the influence of chemistry and transport on N_2O isotope distributions can be interpreted in the framework of a one-dimensional reaction-advection-diffusion regime (Sect. 3.2), or as two-end member mixing relationships (Sect. 3.3). Meridional and seasonal variations in apparent fractionation constants are identified, followed by the discussion of possible mechanisms explaining these variations (Sect. 3.2 to 3.4). We also show that the relationship between different intramolecular isotopic signatures of N_2O varies with altitude, giving insights into the contribution of individual N_2O sinks at different stratospheric levels (Sect. 3.5).

2 Experimental methods

2.1 Sample collection

Upper tropospheric and stratospheric balloon air samples from altitudes between 6 and 34 km were collected at one tropical (Hyderabad/India, 17.5° N), two mid-latitude (Aire sur l'Adour/France, 43.7° N; Gap/France, 44.4° N), and one polar site (Kiruna/Sweden, 67.9° N). We analyzed a total of 132 samples, which were collected using balloon-

borne cryogenic whole air samplers during 12 launches between March 1987 and March 2003. The first eight profiles between 1987 and 1999 were acquired with the air sampler of the former Max Planck Institute (MPI) for Aeronomy, Katlenburg-Lindau/Germany (now: MPI for Solar System Research). The final four profiles were performed by the BONBON air sampler jointly developed by the Research Centre Jülich/Germany and the Institute for Meteorology and Geophysics (now: Institute for Atmosphere and Environment) at the J. W. Goethe University, Frankfurt/Germany. Both air samplers consist of 15 electro-polished stainless steel tubes immersed into liquid neon at a temperature of 27 K, but differ especially in the intake design (see Schmidt et al., 1987, for details). The sampling tubes have an internal volume of about 500 cm^3 and usually contain between 2.5 and 25 dm^3 of sample at standard temperature and pressure (STP), corresponding to pressures between 0.54 and 5.4 MPa at 20°C. The altitude-resolution is about 1 km, sampling latitudes are essentially invariant, and longitude variations can be a few degrees, depending on the prevailing zonal winds during sample collection.

Aircraft samples were collected from the high-latitude research aircraft M55 Geophysica during the EUPLEX (European Polar Stratospheric Cloud and Lee Wave Experiment) campaign in January/February 2003 in Kiruna/Sweden (67.9° N). A total of 88 samples was analyzed for their N_2O isotopic composition. The samples were collected using a new whole air sampler developed at the MPI for Nuclear Physics, Heidelberg/Germany. The sampler uses trace-gas clean metal bellows pumps to collect up to 20 samples into electro-polished stainless steel flasks of 2 dm^3 internal volume. At a pressure of about 0.3 to 0.4 MPa, this gives sample amounts of 6 to 8 dm^3 (STP). The samples span a smaller altitude range (8 to 20 km) than individual balloon profiles, but larger latitude (65.6 to 80° N) and longitude (9.1 to 48.8° E) bands.

Table 1 summarizes sampling dates and locations of all published isotope measurements of stratospheric N_2O, including the 220 samples analyzed for this paper. N_2O is usually zonally well-mixed, but for completeness we show both latitude and longitude of the sampling locations, where available.

2.2 Isotope analysis and measurements of N_2O mixing ratios

The position-dependent isotopic composition of N_2O was measured as described previously (Röckmann et al., 2003b). We assign a locant 1 to the terminal nitrogen atom in N_2O and a locant 2 to the central nitrogen atom, so that the corresponding relative isotope enrichments (δ values) are designated ${}^1\delta^{15}N$ and ${}^2\delta^{15}N$. Other authors are using a locant β for the terminal and α for the central nitrogen atom (Yoshida and Toyoda, 2000). δ values are defined as the relative deviation of the isotope ratio of the sample to a reference isotope ratio:

$$\delta = \frac{R_{\text{sample}}}{R_{\text{reference}}} - 1 \tag{1}$$

The isotope ratio R is defined as the abundance ratio of the heavier isotope and the lighter isotope, i.e., ${}^{15}N$ and ${}^{14}N$ in the case of nitrogen and ${}^{18}O$ and ${}^{16}O$ in the case of oxygen. Variations of the ${}^{17}O/{}^{16}O$ isotope ratio were not measured, but for data reduction purposes, we assume that stratospheric N_2O has the same small relative ${}^{17}O$ excess of $\Delta^{17}O$=0.9‰ as tropospheric N_2O (Kaiser et al., 2003a). This assumption follows theoretical considerations (Kaiser and Röckmann, 2005), but the possible error introduced by this assumption is small because the ${}^{17}O$ correction to the $\delta^{15}N$ values is only about $-0.1\Delta^{17}O$ for ${}^2\delta^{15}N$ and $-0.05\ \Delta^{17}O$ for average $\delta^{15}N=({}^1\delta^{15}N+{}^2\delta^{15}N)/2$.

Generally, the reference isotope ratios are those of air-N_2 for nitrogen and Vienna Standard Mean Ocean Water (VSMOW) for oxygen isotope measurements. However, in the present paper we frequently deviate from this convention and express the stratospheric isotope ratios relative to those of tropospheric N_2O. Thus, the individual isotope signatures are more easily intercomparable. Moreover, assigning a specific position-dependent nitrogen isotope scale is problematic at the present time because two significantly different absolute isotope calibrations exist and the discrepancies have not been resolved yet (Kaiser et al., 2004a; Toyoda and Yoshida, 1999). At times when we interpret our results in the framework of a simple Rayleigh fractionation approach, we

ACPD
6, 4273–4324, 2006

EGU

apply a further normalization by correcting for the temporal trend in the isotope ratio of tropospheric N_2O and the age of stratospheric air (Sect. 3.2). Thus, the isotope profiles for individual years can be compared directly. Furthermore, we can study variations in the ratio between position-dependent isotope signatures for individual samples in order to separate isotope variations due to transport from those due to changing chemistry (Sect. 3.5).

In practice, we base our isotope measurements on a tank of tropospheric N_2O, which was collected on 15 March 2002 at Mount Schauinsland in southwest Germany (SIL-N_2O). Its isotope composition was determined by offline N_2O isotope analysis (Kaiser et al., 2003a) and found to be $\delta^{15}N=(6.6\pm0.1)‰$, $^1\delta^{15}N=(-16.0\pm0.2)‰$, $^2\delta^{15}N=(29.1\pm0.2)‰$ and $\delta^{18}O=(44.6\pm0.1)‰$. In order to avoid large nonlinearity corrections (see Röckmann et al., 2003b), we strove to roughly adjust the extraction time of the trace gas pre-concentration system using a previously measured N_2O mixing ratio value so that the peak area matched that of the Schauinsland reference tank sample (about 4.4 Vs for the N_2O^+ peak, corresponding to 2.0 nmol of N_2O). In cases where the available sample amount was limited, this was not always possible, but even then the necessary non-linearity corrections were at most 0.5‰ for $\delta^{15}N$ and $\delta^{18}O$ and less than 1.5‰ for $^1\delta^{15}N$ and $^2\delta^{15}N$. This concerned samples from the high latitudes and/or altitudes with correspondingly low mixing ratios and high δ values, so that the relative error due to this non-linearity correction is small. For analyses of the N_2O^+ molecular ion, sample sizes ranged from 0.3 to 2.1 nmol (0.5 to 4.6 Vs) with an average of (1.7±0.4) nmol or (3.6±0.9) Vs. For the NO^+ fragment ion, which is used for position-dependent ^{15}N analysis, the range was 1.0 to 7.0 nmol (0.4 to 2.8 Vs) with an average of (4.4±1.0) nmol or (1.7±0.4) Vs. A larger amount of sample was used for NO^+ fragment analysis because the relative abundance of NO^+ in the N_2O mass spectrum is only about 20% of the N_2O^+ molecular ion for the mass spectrometers and ion source configurations we were using.

All isotope analyses were performed on a Finnigan Delta Plus XL isotope ratio mass spectrometer except for the last balloon flight on 6 March 2003, which was analyzed on

a Delta Plus XP mass spectrometer. The Delta Plus XP allows simultaneous registering of mass-to-charge ratios 30, 31, 44, 45, and 46, which has the advantage of requiring only a single extraction/injection of sample for analysis. The reproducibility for a 2 nmol N_2O sample was about 0.15‰ for $\delta^{15}N$ and $\delta^{18}O$ and about 0.5‰ for $^1\delta^{15}N$ and $^2\delta^{15}N$, which is the best precision achieved to date for stratospheric N_2O samples (Park et al., 2004; Toyoda et al., 2004).

Mixing ratios (μ) were calculated by comparing the extraction time-weighted peak areas of the stratospheric samples with those of the Schauinsland reference tank samples. The N_2O mixing ratio of the Schauinsland reference tank was determined by Ingeborg Levin at the Institute for Environmental Physics, Heidelberg/Germany, using GC-ECD (gas chromatography-electron capture detection) and found to be (319.0±0.2) nmol/mol (SIO98 scale; Prinn et al., 2000). N_2O mixing ratios were derived both from NO^+ fragment and N_2O^+ molecular ion peak areas. Figure 1 shows that they follow a 1:1 relationship very closely, with the NO^+-derived mixing ratio being on average (1.3±2.1) nmol mol^{-1} higher. We adopt the mean of the N_2O^+- and the NO^+-derived mixing ratio as the mixing ratio of the individual sample. For a subset of 47 samples, we have compared this mixing ratio to independent GC-ECD measurements at the Institute for Meteorology and Geophysics of the University of Frankfurt (Fig. 2). The average relative difference is (−0.3±2.1)%, with relative differences of 1% or smaller for larger mixing ratios and larger relative differences for smaller mixing ratios. Thus, precision and accuracy of the mixing ratio measurements by mass spectrometry are sufficient for the derivation of apparent fractionation constants in the stratosphere with an uncertainty of about 1%.

3 Results and discussion

We start this section with a general description of the balloon profiles in terms of their mixing ratios and then proceed to explore the variation of the isotopic composition with the mixing ratio. In a first step, we will interpret the data in a Rayleigh fractionation

framework, as applied in past studies of stratospheric N_2O (Griffith et al., 2000; Park et al., 2004; Rahn and Wahlen, 1997; Röckmann et al., 2001; Toyoda et al., 2001). As a second step and partly in response to a question raised by Park et al. (2004), we explore to what extent simple end-member mixing can describe the co-variation between isotope and mixing ratios and whether a more complex "continuous weak mixing" scheme (Plumb et al., 2000) can give a better description for part of the data. Finally, we investigate whether correlations between N_2O isotope signatures are useful indicators of the partitioning between $O(^1D)$ and photolytic N_2O sinks and of changes of temperature and actinic fluxes with altitude.

3.1 N_2O mixing ratios

Figure 3 shows vertical profiles of the N_2O mixing ratio. The decrease of tropopause altitude, z_{trop}, from the low-latitude Indian samples (z_{trop}≈16 km) to the polar Kiruna samples (z_{trop}≈7 km) can be estimated from the point where the mixing ratio starts to drop below its tropospheric value of 310 to 320 nmol mol^{-1}. Correspondingly, the profiles can be separated into those of polar character (all Kiruna profiles except for the high altitude-samples of the Kiruna 03/95 profile), mid-latitude character (Gap 06/99, all Aire sur l'Adour profiles, and the high-altitude Kiruna 03/95 samples) and tropical character (India profiles). The Kiruna profiles were obtained in winter and generally sampled air from inside the polar vortex, although the distinction between polar and mid-latitude samples is only unambiguous for mixing ratios below 290 nmol mol^{-1}. In contrast, the polar vortex had already broken up completely by the time of the 03/95 balloon launch and the resulting N_2O profile corresponds to a mid-latitude one. The distinction between tropical and mid-latitude samples can be made most clearly for mixing ratios above 250 nmol mol^{-1}, but some overlap occurs for lower mixing ratios.

The above classification based on the vertical N_2O profiles is rather crude and sensitive to intra- and interannual synoptic changes of the large-scale stratospheric circulation. Correlations between different stratospheric trace gases are better suited to

segregate the stratosphere into regions because characteristic tracer-tracer relationships develop in areas where exchange time-scales due to transport and mixing are significantly shorter than the instantaneous chemical lifetimes. Michelsen et al. (1998) developed an N_2O-CH_4 climatology with polynomial fits for different stratospheric regions and we show our data in context of these fits in Fig. 4. No clear separation into stratospheric regions is possible for N_2O mixing ratios above 150 nmol mol^{-1}, but below this value, the picture that developed from the vertical N_2O profiles is confirmed with one exception: The 140 nmol mol^{-1} sample obtained from the India 04/99 launch clearly stands out as a tropical N_2O sample, whereas the India 03/87 samples rather show mid-latitude character. This is in line with historic CH_4 profile variations, which showed that the intertropical convergence zone (ITCZ) moves northward across the sampling location of Hyderabad between end of March and end of April, but was still south of Hyderabad on 26 March 1987 (Patra et al., 2003). Some caution is warranted in the interpretation of our data in context of these CH_4-N_2O relationships because the latter have been derived with data from the years 1993 and 1994 (Michelsen et al., 1998), but will change in time due to the different relative growth rates of atmospheric N_2O and CH_4 of 0.25%/a and between 0 and 0.8%/a, respectively (Prather et al., 2001). This may explain why the India 03/87 samples fall below the generic tropical N_2O-CH_4 climatology.

3.2 Isotope variations in a Rayleigh fractionation framework

Figure 5 shows the relationship between average $\delta^{15}N$ values (relative to SIL-N_2O) and N_2O mixing ratios. The isotopic enrichment generally increases with decreasing mixing ratios due to the increasing degree of photochemical removal of N_2O and the associated kinetic isotope effects, which lead to preferential destruction of the lighter isotopologues. Samples with mixing ratios above 200 nmol mol^{-1} display a uniform compact relationship independent of latitude, which was also noted by Park et al. (2004). However, samples with μ<200 nmol mol^{-1} clearly split up into different profiles, depending on latitude and sampling season. Mid-latitude samples collected in fall maintain a

rather compact relationship even below 200 nmol mol^{-1}. However, samples from polar latitudes (Kiruna) and the mid-latitude summer profile (Gap 06/99) differ substantially among each other and from the fall mid-latitude profiles. Notably, the Kiruna 03/95 profile, which was classified as a mid-latitude profile based on its CH_4-N_2O correlation and the shape of the vertical N_2O profile, falls below the ASA fall profiles. It is similar to the Gap 06/99 summer profile, though. The polar vortex samples show $\delta^{15}N$ variations of more than 25‰ for the same N_2O mixing ratio, which means that the photochemical and transport processes that establish the mid-latitude δ-μ relationship do not prevail in the polar vortex. This is due to dynamic isolation of the polar vortex and the limited degree of photochemical processing that occurs over the dark polar areas. In addition, mixing with upper stratospheric and/or mesospheric air (Sect. 3.3) as well as more complicated mixing processes (Sect. 3.4) can play a role.

For illustrative purposes, Fig. 5 also shows two hypothetical Rayleigh fractionation lines, which have been calculated assuming a closed system with no sources and a single sink with an isotope effect ε of −38.0‰ and −19.2‰, respectively. Rayleigh fractionation then leads to $\delta=(\mu/\mu_T)^{\varepsilon}-1$. The two limits for ε correspond to an intrinsic photochemical isotope effect as expected from broadband photolysis at room temperature with a 10% contribution from N_2O photo-oxidation and the apparent isotope effect expected for transport-limited conditions (about half the intrinsic isotopic effect) (Kaiser et al., 2002a, b). These upper and lower bounds delimit the range of isotope effects, which can be realized in a purely one-dimensional reaction-advection-diffusion system at steady-state. This was demonstrated for the reaction-diffusion system (Kaiser et al., 2002a; Kaye, 1987; Morgan et al., 2004), but is still valid even if advection is included due to the linearity of the corresponding differential equation (Kaiser and Röckmann, 2006[1]). As noted in most previous publications on stratospheric N_2O isotopes (e.g., Rahn et al., 1998; Röckmann et al., 2001; Toyoda et al., 2001), the stratospheric mea-

[1]Kaiser, J. and Röckmann, T.: Apparent isotope effects in atmospheric and oceanic environments, in preparation, 2006.

surements clearly fall below the $\delta-\mu$ relationship defined by the intrinsic isotope effect, which is due to transport and mixing effects. The magnitude of the intrinsic isotope effect used here is only an estimate because, on the one hand, the photolytic isotope effect is larger at lower (stratospheric) temperatures (Kaiser et al., 2002b; von Hessberg et al., 2004) and, on the other hand, the contribution of the photo-oxidation sink may vary (Sect. 3.5). In any case, a simple Rayleigh model fails to describe the measurements. For mixing ratios below 70 nmol mol^{-1}, the attenuation of the intrinsic isotope effect due to diffusion and advection can explain this discrepancy because the observations lie mostly above the apparent fractionation constant under transport-limited conditions. However, at mixing ratios greater than 70 nmol mol^{-1}, some δ values are even smaller than expected for the one-dimensional, transport-limited case. This means that other effects such as mixing have to be invoked the explain the observations (see Sect. 3.3). It should also be noted that the above analysis is simplified in the sense that it uses only tropospheric N_2O mixing ratios and δ values as initial conditions for the Rayleigh fractionation approximation and does not consider variations of the fractionation constant as N_2O gets depleted. A more appropriate approach will therefore be used in the following section, in which we use the local slope in a Rayleigh fractionation plot to estimate the apparent fractionation constant.

3.2.1 Corrections for atmospheric trends and stratospheric age of air

For a quantitative analysis of the observed δ values in a Rayleigh fractionation framework, we have to apply corrections for the time of sampling (the samples span a range of 16 years) and the age of stratospheric air. In order to make the different profiles intercomparable, we first adjust the measured isotopic compositions to a specific date in order to correct for the changing isotopic composition of modern atmospheric N_2O. Due to anthropogenic inputs of isotopically light N_2O, the δ values are decreasing with time, as deduced from analyses of Antarctic firn air (Bernard et al., 2006; Röckmann et al., 2003a; Sowers et al., 2002) and direct atmospheric measurements (Röckmann and Levin, 2005). As a base date, we arbitrarily chose the sampling date of the

SIL-N_2O reference tank (15 March 2002). The correction we apply is based on recent direct measurements of the position-dependent isotope composition of archived, clean southern hemisphere background air samples collected at the German Antarctic "Georg von Neumayer" Station (70°39′ S, 08°15′ W). Röckmann and Levin (2005) found linear trends of (−0.040±0.003)‰/a for $\delta^{15}N$, (−0.064±0.016)‰/a for $^{1}\delta^{15}N$, (−0.014±0.016)‰/a $^{2}\delta^{15}N$, and (−0.021±0.003)‰/a for $\delta^{18}O$ over the time-span of available samples (between March 1990 and November 2002). We assume that these linear trends were constant over the time-span defined by the stratospheric samples (March 1987 to March 2003).

In order to investigate the influence of transport and chemistry on the isotopic composition of stratospheric N_2O, we linearize our data in a Rayleigh fractionation plot of $\ln(1+\delta)$ vs. $\ln(\mu/\mu_T)$ (The error due to using N_2O rather than $^{14}N^{16}_{2}O$ mixing ratios can be neglected; see Kaiser et al., 2002a). The local slope then corresponds to an apparent fractionation constant. To pursue this approach as accurately as possible, we have to estimate μ_T, the N_2O mixing ratio at the tropopause when the air parcel entered the stratosphere, and apply a further correction to δ to take the age of air into account. These corrections are small relative to the measurement error (usually <1%), but were deemed necessary in order to achieve a closer analogy to a Rayleigh fractionation system. Therefore, we consider the age of stratospheric air in order to normalize all data to a single stratospheric entry datum. The age of air is defined as the time elapsed since an air parcel has passed the tropopause. We base our age-of-air estimate on the relationship between N_2O mixing ratios and the age of mid-latitude/lower polar vortex air found by Boering et al. (1996) for samples from the years 1992 to 1996. A polynomial regression of the age of air Γ versus μ/μ_T gives $\Gamma(\mu/\mu_T)/a=-(7.43\pm0.34)\ (\mu/\mu_T)^3+(3.68\pm0.56)\ (\mu/\mu_T)^2-(1.94\pm0.28)\ \mu/\mu_T+5.69\pm0.04$ (R^2=0.998), with the tropopause mixing ratio μ_T adjusted to 311.6 nmol mol^{-1} to give an age of zero for $\mu=\mu_T$. The value of 311.6 nmol mol^{-1} agrees with AGAGE observations at the northern hemisphere background station Mace Head/Ireland in 1994. However, given the time range of observations (1992 to 1996), the global extent of

sampling locations used by Boering et al. (1996) and the age difference of tropopause air relative to tropospheric air, one might have expected a slightly lower value than 311.6 nmol mol^{-1}. The difference might be due to different N_2O calibration scales. The use of μ/μ_T for the Γ parameterization rather than μ itself minimizes errors due to the increase of the N_2O mixing ratio with time. The parameterization will differ slightly for polar and tropical samples, but the differences only lead to second-order corrections for the present application and can be neglected. Engel et al. (2002) have derived a similar third-order polynomial regression of Γ versus the N_2O mixing ratio. The age differences to the parameterization based on the data of Boering et al. (1996) are at most 4 months, which can be neglected for the present application.

We use the estimated age of air and assume that the age difference between tropopause and tropospheric air is 0.8 years (Volk et al., 1997). We then calculate the isotopic composition of the stratospheric sample relative to its composition when it left the tropopause, using the same isotope trends as above (Röckmann and Levin, 2005). Similarly, we estimate the tropopause N_2O mixing ratio for individual samples. The northern-hemisphere AGAGE data from Mace Head (Ireland) are used as reference for the correction because all our data are from the northern hemisphere. Second-order effects due to intrahemispheric N_2O mixing ratio gradients are neglected. For the pre-AGAGE period before 1994, we use the GAGE data from Cape Grim (Australia) instead because they display more consistent interannual variations and a cleaner seasonal signal than the GAGE data from Mace Head record. In order to account for interhemispheric N_2O mixing ratio differences, the Cape Grim data are time shifted forward by 0.8 months and adjusted upward by 0.7 nmol mol^{-1}. This adjustment is based on a comparison between the AGAGE data from Cape Grim and Mace Head for the years 1994 to 2002.

3.2.2 Calculation of ε_{app} from global fits and local slopes

Using the corrected N_2O isotope and mixing ratios, apparent fractionation constants (ε_{app}) can be calculated from $\ln(1+\delta)$ and $\ln(\mu/\mu_T)$ (Fig. 6). We use two different ap-

proaches to do this. First, we calculate average linear least-squares ε_{app} values for individual lower stratosphere profiles using only samples with $\ln(\mu/\mu_T) > -0.6$. An $\ln(\mu/\mu_T)$ value of −0.6 corresponds to N_2O mixing ratios between 168 and 174 nmol mol^{-1} for the age range of our samples. The same cut-off has already been used by Kaiser (2002) and von Hessberg et al. (2004) and corresponds to the region of the Rayleigh fractionation plot without noticeable curvature. Below $\ln(\mu/\mu_T)$ values of −0.6, the Rayleigh fractionation plots show positive curvature and a linear fit is therefore no longer appropriate. Instead, we fit a second-order polynomial to the individual profiles and calculate local slopes from the first derivative of the fit at exemplary $\ln(\mu/\mu_T)$ values of −1.0, −1.5 and −2.0. This serves to illustrate how ε_{app} values change for higher altitude samples. We exclude samples with $\ln(\mu/\mu_T) < -2.4$ from the fit because these samples are influenced by mixing with low-N_2O upper stratospheric and mesospheric air (Sect. 3.3). Compared to previous studies, in which linear fits were both applied to the middle and to the lower stratospheric samples (Kaiser, 2002; Park et al., 2004; Toyoda et al., 2001, 2004), our present approach has the advantage to expose differences between individual profiles more clearly and to decrease the influence of the highest-enriched samples on the overall fit.

3.2.3 Vertical and meridional trends in ε_{app}

The apparent Rayleigh fractionation constants we derive according to the two approaches described above are shown in Table 2 and, for $\varepsilon^{15}N$, in Fig. 7 as a function of latitude (the trends look qualitatively the same for other N_2O isotope signatures due to their high correlation, see Sect. 3.5). In general, the magnitude of ε_{app} increases with altitude and decreases with increasing distance from the equator. The latter relationship is what one would expect qualitatively for faster vertical transport time-scales near the equator (photochemistry is rate-limiting). This effect outweighs the faster photolysis rates due to higher actinic fluxes at low latitudes. However, the increase of the magnitude of the apparent fractionation constant with altitude is opposite to what one would expect from a simple vertical reaction-diffusion-advection model (Kaiser, 2002; Toyoda

et al., 2004). Despite the conceptual usefulness of this one-dimensional description, it has to be stressed that stratospheric transport cannot be characterized as a function of altitude only and that vertical diffusion is actually not an important process, even though it can be helpful to describe stratospheric transport to some extent. Meridional transport schemes have to be included to explain the variation of ε_{app}. Possible schemes based on mixing processes are discussed in Sect. 3.3.

Specifically, average $\varepsilon^{15}N_{app}$ values at $\ln(\mu/\mu_T) > -0.6$ are about −19‰ at tropical latitudes, −17‰ at mid-latitudes and −15‰ at polar latitudes. This is clearly less than half the intrinsic fractionation constant of about $^1/_2$ (−50‰) at a lower stratospheric temperature of 217 K (Kaiser et al., 2002b), estimated from broadband N_2O photolysis with an ultraviolet (UV) lamp that simulates the solar spectrum at stratospheric altitudes. The influence of spectral UV irradiance variations with altitude on the photolytic fractionation constant is small (Kaiser et al., 2003b). The discrepancy to the observations can be explained by at least a 25% contribution of photo-oxidation to the total N_2O sink or by mixing effects other than vertical diffusion. Toyoda et al. (2004) based their analysis of the diminished apparent fractionation constants compared to their intrinsic values on photo-oxidation only, which led to estimated contributions of photo-oxidation between 70 and 80% to the total sink. However, this analysis is flawed because reductions of the intrinsic fractionation constant due to vertical diffusion and mixing were neglected. In Sect. 3.5, we show that correlations between isotope signature do indicate an unambiguous contribution of photo-oxidation, but to a much lesser degree than 70%.

As already mentioned, $|\varepsilon_{app}|$ increases with altitude, but even at middle stratospheric altitudes ($\ln(\mu/\mu_T) = -2.0$), $\varepsilon^{15}N_{app}$ values are far below −48‰, corresponding to photolytic fractionation constants at temperatures of about 233 K (Kaiser et al., 2002b). $|\varepsilon_{app}|$ is usually above half the intrinsic fractionation constant, in line with simulated values based on vertical eddy diffusion coefficients and N_2O destruction rates (Kaiser, 2002; Kaiser et al., 2002a; Toyoda et al., 2004).

3.2.4 Seasonal trends in ε_{app}

Seasonal trends in the apparent fractionation constants are difficult to discern (Table 2), because the available balloon profiles are biased towards specific months, even if we combine our data-set with that of Toyoda et al. (2004). The two tropical profiles are both from spring, and the polar profiles are from winter/early spring. Only the mid-latitude profiles allow for a limited comparison between late spring/summer and autumn. The Gap 06/99 profile shows generally smaller $|\varepsilon_{app}|$ values than the fall ASA profiles. This is in contrast to model simulations by Morgan et al. (2004) that did not show variations in ε_{app} at mid-latitudes. However, the simulations did show variations at polar and tropical latitudes, which were attributed to transport effects. Therefore, we tentatively associate the observed variations at mid-latitudes with transport effects as well.

Similar variations were observed by Toyoda et al. (2004) for balloon profiles acquired over Japan. For example, in a plot of isotope versus mixing ratios (not shown), the Sanriku 08/00 and 09/98 profiles behave similar to the ASA 09/93, 10/01 and 09/02 samples (late summer/fall), whereas the Sanriku 05/99, 05/01 and 06/90 profiles bear closer resemblance to the Gap 06/99 profile and the polar samples (spring/early summer). Modeling attempts therefore have to consider seasonal and meridional variations of the N_2O isotope signature if quantitative agreement with observations is to be achieved. However, it might even be necessary to include longitudinal variations as a comparison between the Gap 06/99 and Sanriku 05/99 profiles shows (Fig. 8). Both profiles were obtained at nearly the same time of the year (three weeks apart) and nearly the same latitude (44° N and 39° N), but nevertheless show distinct differences especially in the middle stratosphere.

3.3 Influence of end-member mixing on N_2O isotope ratios

In our data interpretation so far, we have focused on vertical diffusive effects on the apparent fractionation constants. However, meridional transport and mixing can also influence the observed relationship between N_2O isotope signatures and mixing ratios

(Kaiser et al., 2002a). Specifically, Park et al. (2004) mentioned two mixing scenarios, "end-member mixing" and "continuous weak mixing" (Plumb et al., 2000), in the context of $\delta-\mu$ relationships for the polar vortex. In the following, we will investigate to what degree these scenarios can explain the observed stratospheric N_2O isotope profiles, not only in the polar vortex, but also in other stratospheric regions. We start with "end-member mixing", followed by "continuous weak mixing", with a short mathematical introduction to each scheme.

3.3.1 Theory

"End-member mixing" corresponds to the mixing of two air masses in different relative volumetric ratios. It is "linear" in terms of concentrations; however, δ values have to be weighted by the corresponding concentrations. Mathematically, this can be expressed by the following relationships for two air masses, A and B (Kaiser et al., 2002a):

$$c = x_A c_A + (1 - x_A) c_B \tag{2}$$

$$c\delta = x_A c_A \delta_A + (1 - x_A) c_B \delta_B \tag{3}$$

The symbol x designates a volumetric air mass fraction, the symbol c designates concentrations. Indices denote the air mass. Non-indexed symbols correspond to the mixed air mass. If both air masses have the same density, mixing ratios (μ) can be used instead of concentrations. This condition is assumed to be always valid, because both air masses have to be at the same altitude in order to mix. Therefore, we replace concentrations by mixing ratios and solve Eq. (2) for x:

$$x = \frac{\mu_B - \mu}{\mu_B - \mu_A}, \tag{4}$$

which is then substituted into Eq. (3) and solved for δ:

$$\delta = \frac{\mu_B - \mu}{\mu_B - \mu_A} \frac{\mu_A \delta_A}{\mu} + \frac{\mu - \mu_A}{\mu_B - \mu_A} \frac{\mu_B \delta_B}{\mu}$$

$$= \frac{\mu_B \delta_B - \mu_A \delta_A}{\mu_B - \mu_A} + \frac{\delta_B - \delta_A}{\mu_B^{-1} - \mu_A^{-1}} \frac{1}{\mu} \quad (5)$$

Thus, end-member mixing should lead to linear relationships between δ values and inverse mixing ratios ($1/\mu$). This kind of plot is better suited to diagnose mixing than $\delta - \mu$ plots (Park et al., 2004), because both mixing and Rayleigh fractionation appear as similar non-linear curves in a $\delta - \mu$ plot. Note that after correction for a sign error, Eq. (8) derived for oceanic O_2 in Bender (1990) corresponds to Eq. (5) above.

3.3.2 Evidence for mixing from balloon samples

Without restriction of generality, we develop our analysis using $\delta^{15}N$ (the other isotope signatures behave very similarly, see Sect. 3.5). The $\delta^{15}N$ values of the present stratospheric dataset have been plotted versus their inverse mixing ratios in Fig. 9. Most of the samples cluster near the origin of the plot. At this scale, the tropical, mid-latitude ASA and low-altitude polar samples follow a linear relationship. However, the mid-latitude Gap 06/99 and the high-altitude polar samples deviate from this linear relationship at mixing ratios below 180 nmol mol^{-1}. Contrary to the suggestion of Park et al. (2004), the behavior of the latter samples cannot be explained by simple end-member mixing because they do not describe a linear array in $\delta - \mu^{-1}$ space.

Figure 10 shows the same data as in Fig. 9 restricted to mixing ratios above 50 nmol mol^{-1}. Again, the non-linearity of the δ vs. μ^{-1} relationship for polar samples is apparent, while the mid-latitude ASA samples nearly follow a linear relationship down to mixing ratios of 60 nmol mol^{-1}. The green line in Fig. 10 shows a linear fit to the ASA 09/93 data, $\delta^{15}N(\text{ASA 09/93}) = 4.0 \cdot 10^{-9}\ \mu^{-1} - 12.4‰$ ($R^2 = 0.997$). This indicates that the mid-latitude N_2O isotope profiles could be described by a simple end-member mixing relationship, to a good degree of approximation. The advantage of using the relationship between δ and the inverse mixing ratio to diagnose mixing is that it is based on the photochemistry of a single trace gas only. If transport is fast with respect to photochemistry of N_2O, then linear mixing relationships between δ and μ^{-1} result. In

contrast, CH_4–N_2O correlations are only linear if transport is fast with respect to the chemistry of both trace gases. This may explain why the mid-latitude samples follow an end-member mixing relationship closely in δ–μ^{-1} space, but not in CH_4–N_2O space (Fig. 4). Nevertheless, the linearity of the δ–μ^{-1} relationship is not perfect and the scatter about the linear regression line is significantly larger than the analytical errors. It must therefore be due to natural variability. Moreover, even the mid-latitude ASA samples show a decrease in the slope towards lower mixing ratios, which indicates that – despite the strong correlation between δ and μ^{-1} – it cannot be end-member mixing alone that is responsible for the mid-latitude N_2O isotope profile.

3.3.3 Evidence for mixing from aircraft samples

Figure 10 also shows two dense data-sets from aircraft campaigns into and out of the Arctic polar vortex (SOLVE 2000; see Park et al., 2004; and EUPLEX 2003). Again, for mixing ratios above about 200 nmol mol^{-1}, δ follows a linear relationship relative to μ^{-1}. However, overall the relationship is curved. E.g., for EUPLEX 2003, the δ^{15}N values can be approximated by a second-order polynomial: δ^{15}N(EUPLEX 2003)=$-1.4{\cdot}10^{-16}\,\mu^{-2}+4.9{\cdot}10^{-9}\,\mu^{-1}-14.2$‰ ($R^2$=0.998). Neither linear mixing nor Rayleigh fractionation can explain the observed behavior at mixing ratios below 200 nmol mol^{-1}. A different transport scheme must therefore be invoked, possibly "continuous weak mixing" (Sect. 3.4).

Figure 11 demonstrates this behavior in greater detail. The left panel shows the residual for the EUPLEX 2003 and SOLVE 2000 data after a linear least-squares fit has been applied to the data between 200 and 320 nmol mol^{-1}. The right panel shows an analogous fit of the data between 170 and 320 nmol mol^{-1}. In both cases, the residuals become very large below the lower boundary of the fit region. However, in the 170 nmol mol^{-1} case, the residuals also show a pattern in the range between 170 and 320 nmol mol^{-1}, with foremost positive residuals in the 170 to 260 nmol mol^{-1} range and negative residuals in the 260 to 320 nmol mol^{-1} range. Such a pattern is absent in the 200 nmol mol^{-1} range. This neatly demonstrates the suitability of linear

mixing to describe the lower polar vortex relationship between N_2O mixing ratios and isotope ratios, for mixing ratios above approximately 200 nmol mol^{-1}.

As noted above, a Rayleigh plot yields a linear array in $\ln(1+\delta)-\ln(\mu/\mu_T)$ space, for $\ln(\mu/\mu_T)>-0.6$, corresponding to mixing ratios >160 nmol/mol, so that the correlation between δ and μ for mixing ratios >200 nmol mol^{-1} could potentially be explained by Rayleigh fractionation under the influence of vertical advection and diffusion. However, the slope of a linear fit to the Rayleigh plot is smaller even than the reduced fractionation constant under diffusion-limited conditions, i.e. half the value of the intrinsic fractionation constant, and this simple explanation model alone is therefore not sufficient.

The failure of "end-member mixing" to describe the N_2O isotope variations in polar aircraft samples with N_2O mixing ratios below about 200 nmol mol^{-1} can be interpreted as a hint to the mechanism by which upper stratospheric air in the polar vortex mixes with extra-vortex mid-latitude air. Rather than a single, "late" mixing event, "continuous weak mixing" between vortex and extra-vortex air might be the relevant mechanism. This process was first proposed and developed conceptually by Plumb et al. (2000). In Sect. 3.4, we include isotopes in a two-dimensional transport scheme similar to the one used by Plumb et al. and evaluate whether the observed isotope variations could indeed be due to continuous weak mixing.

3.3.4 Upper stratospheric or mesospheric air intrusions

Figures 9 and 10 also show that polar balloon samples with N_2O mixing ratios below 100 nmol mol^{-1} strongly deviate from the mid-latitude $\delta-\mu^{-1}$ relationship, especially in the case of the Kiruna 03/03 profile. The latter profile comprises three samples with mixing ratios between 7 and 19 nmol mol^{-1}, but nearly identical $\delta^{15}N$ values around 60‰. They were obtained at altitudes of 23.9 km (7 nmol mol^{-1}), 25.3 km (13 nmol mol^{-1}), and 28.4 km (19 nmol mol^{-1}). The nearly horizontal array of these three samples in $\delta-\mu^{-1}$ space can be explained by mixing with N_2O-free upper strato-

spheric or mesospheric air, descending diabatically in the polar vortex, as was first suggested by Toyoda et al. (2004). In the polar night, no photochemical destruction of N_2O occurs and transport is therefore the only process that can influence the relationship between N_2O isotope and mixing ratios. The fact that the high-latitude Kiruna 03/03 samples contained mesospheric air was first established by CO_2 and SF_6 analyses of the same set of samples analyzed here (Engel et al., 2006). Meteorological observations and age of air estimates derived from these trace gas measurements showed that in the boreal winter of 2002/2003, there was indeed an mesospheric intrusion into the Arctic polar vortex, which descended in the vortex throughout the winter. Based on Fig. 9, a similar event must have occurred in the winter of 1992.

3.4 Influence of continuous weak mixing on N_2O isotope ratios

Plumb et al. (2000) showed that tracer-tracer relationships in the Arctic vortex are better interpreted by continuous weak mixing across the vortex than by simple end-member mixing. They used a conceptual two-dimensional model to illustrate the effects of continuous mixing and showed that compact tracer-tracer relationships develop for exterior air and vortex air, with a small transition region in between. We have used the same conceptual model as Plumb et al. (2000) to investigate whether continuous mixing is a useful concept to better interpret the isotope variations in our polar vortex samples.

Briefly, a simple advective-diffusive model in cylindrical geometry is set up with 41 grid points in the r-direction and 101 grid points in the z-direction, corresponding to latitude and altitude. Latitudinal downwelling with vertical velocity $w(r)=-\cos(1/2\pi r)$ is assumed, so that the maximum downwelling occurs at the pole (note the correction of a typo in the definition of w in Plumb et al., 2000). The model is dimensionless with spatial co-ordinates from 0 to 1 and mixing ratios expressed relative to their value at the tropopause ($\chi=\mu/\mu_T$). The unit of time is the time it takes for air to descend at the pole from top to bottom of the domain. With K being the horizontal (eddy) diffusivity,

the normalized mixing ratios evolve according to

$$\frac{\partial \chi}{\partial t} = -w\frac{\partial \chi}{\partial z} + \frac{1}{r}\frac{\partial}{\partial r}\left(rK\frac{\partial \chi}{\partial r}\right).$$

The horizontal diffusivity K was defined by Plumb et al. (2000) as piecewise uniform over several regions (numerical values correspond to the first case discussed in Plumb et al., 2000):

Vortex	$z>0.2$	$r<0.3$	$K=K_v=0.25$
Edge region	$z>0.2$	$0.3<r<0.4$	$K=K_e=0.05$
Exterior		$r>0.4$	$K=K_m=2.0$
Subvortex	$0.1<z<0.2$	$r<0.3$	K: linear transition between K_m and K_v
Subvortex	$1<z<0.2$	$0.3<r<0.4$	K: linear transition between K_m and K_e
Subvortex	$z<0.1$	$r<0.4$	$K=K_m$

We use continuously defined horizontal diffusivities instead with the same transition points at r=0.3, r=0.4 and z=0.1 as in Plumb et al. (2000):

$$K_r(r)=(K_v-K_e)e^{-(r+0.7)^{38}}+(K_m-K_e)\,e^{-(r-1.4)^{62}}+K_e$$

$$K_r(r,z)=(K_r-K_m)e^{-(z-1.1)38}+K_m$$

As boundary conditions at the exterior edge of the domain (r=1), we set $\chi(1,z)=1/2[\cos(\pi z^2)+1]$, at the bottom $\chi(r,0)=1$ and at the top $\chi(r,1)=0$. At r=0, we specify $\partial\chi/\partial r=0$. For the sake of argument, we assume that the mixing ratio of

ACPD
6, 4273–4324, 2006

the minor isotope at the exterior edge is given by $\chi'(1,z)=\chi(1,z)^{1+\varepsilon}$ with $\varepsilon=-38‰$ (corresponding to the ^{15}N isotope effect used in Figs. 5 and 6).

The resulting steady-state dependence of the isotope ratio on $\chi=\mu/\mu_T$ is shown in Fig. 12. Two compact $\delta-\mu/\mu_T$ relationships of finite width develop in the vortex and in the exterior, just as found by Plumb et al. (2000) for conceptual tracer-tracer relationships between NO_y–N_2O and $CFCl_3$–N_2O. A horizontal (quasi-isentropic) cross-section at $z=0.7$ clearly shows a different $\delta-\mu/\mu_T$ relationship than expected for end-member mixing. The modeled tracer-tracer relationships can also be evaluated in a Rayleigh plot (Fig. 13a) or as mixing plot (Fig. 14a). The Rayleigh plot (Fig. 13a) for a constant value of r bears some similarity to a Rayleigh fractionation plot for a one-dimensional reaction-diffusion-advection scheme with an isotope effect below the intrinsic isotope effect although in the present case no chemistry takes place in the model region. The mixing plot (Fig. 14a) shows that continuous weak mixing leads to curved quasi-isentropic arrays in a $\delta-\mu^{-1}$ plot, which does suggest that the polar N_2O isotope profiles are more likely caused by continuous weak mixing than by end-member mixing.

A comparison of the continuous weak mixing model with stratospheric measurements (Figs. 12b, 13b, and 14b) shows that it captures the features in the stratospheric N_2O isotope data for mixing ratios above 200 nmol mol^{-1}, just as the other two conceptual models discussed here (modified Rayleigh fractionation in a one-dimensional reaction-diffusion-advection scheme and end-member mixing). However, only the continuous weak mixing model seems to simulate the qualitative behavior at both high and low mixing ratios. Modified Rayleigh fractionation leads to linear correlations between $\ln(1+\delta)$ and $\ln(\mu/\mu_T)$. It thus fails to simulate the curvature of the EUPLEX measurements. End-member mixing should yield linear correlations between δ and μ^{-1}, and thus fails at mixing ratios below 200 nmol mol^{-1}. In contrast, in the continuous weak mixing model even the increase of the magnitude of the apparent fractionation constant with decreasing N_2O mixing ratio is noticeable, which means that this conceptual transport model can go a long way towards explaining the observed stratospheric N_2O

isotope variations. This does not mean that the conceptual model presented here should be construed as an attempt to realistically simulate stratospheric transport and chemistry. It only serves to illustrate that the level of precision we have achieved in stratospheric N_2O isotope measurements warrants moving beyond simple Rayleigh fractionation and end-member mixing models. For a full appraisal of the observations two- or three-dimensional atmospheric chemistry models are needed and are in fact already being used (McLinden et al., 2003; Morgan et al., 2004).

3.5 Correlations between position-dependent isotope enrichments

In this final section, we demonstrate that position-dependent N_2O isotope measurements are not only useful to make inferences about stratospheric transport, but also bear some signal of variations in the relative contributions of the two photochemical N_2O sinks in the stratosphere, photolysis and reaction with $O(^1D)$, as first suggested by Röckmann et al. (2001) and Toyoda et al. (2001) and further elaborated by Kaiser et al. (2002a, b, 2003b). The effects of transport and mixing on the correlation between apparent fractionation constants essentially cancel (Kaiser et al., 2002a). This can be exploited to discern variations in stratospheric chemistry with respect to altitude or latitude. Based on their data-set of polar aircraft samples, Park et al. (2004) questioned the possibility to detect altitude variations in the relative contribution of the photolysis and $O(^1D)$ sink, but proposed instead that meridional differences in the correlation between different isotope signatures might be apparent, with a stronger influence of the $O(^1D)$ sink at tropical latitudes.

Toyoda et al. (2004) calculated the contribution of the $O(^1D)$ sink from apparent stratospheric fractionation constants and the fractionation constants measured for UV photolysis and the reaction of N_2O with $O(^1D)$ in the laboratory. However, they did not allow for transport effects and the ensuing reduction of the apparent fractionation constant from its intrinsic (i.e., photochemical) value. This led them to conclude erroneously that the contribution of photolysis to the total N_2O sink is significantly less than the value of 90% derived from integrating stratospheric chemistry models (Min-

schwaner et al., 1993). Toyoda et al. (2004) indicated that their dataset was not comprehensive enough to use correlations between individual N_2O isotope signatures to derive the contribution of different photochemical N_2O sinks.

With the present comprehensive, high-precision dataset, we are now revisiting the suggested variations of η, i.e., the correlation between $\ln(1+{}^2\delta^{15}N)$ and $\ln(1+{}^1\delta^{15}N)$, and ψ, i.e., the correlation between $\ln(1+\delta^{15}N)$ and $\ln(1+\delta^{18}O)$ (Kaiser, 2002; Kaiser et al., 2002a; Park et al., 2004). Instead of taking the ratio of apparent fractionation constants over larger stratospheric regions (Röckmann et al., 2001; Toyoda et al., 2004), the large number of available samples now allows pursuing an approach with higher resolution. We compute η and ψ values directly for each individual sample, using the isotope values normalized to a single tropopause date of 15 March 2002. Using η and ψ specifically in this combination of isotope signatures as chemical fingerprints ensures that quantities with comparable errors are combined, in order to minimize statistical errors. By plotting $\ln(1+{}^2\delta^{15}N)$ vs. $\ln(1+{}^1\delta^{15}N)$ and $\ln(1+\delta^{15}N)$ vs. $\ln(1+\delta^{18}O)$, it was verified that there are no significant offsets from the origin for samples with low enrichments, which means that the normalization procedure has effectively removed all artifacts, which might otherwise be present in the computed η and ψ values. The results were then binned in 25 nmol/mol intervals and are shown in Fig. 15.

At high N_2O mixing ratios, both η and ψ show low values, which approach the values expected for photo-oxidation alone (0.25 and 0.5 (Kaiser et al., 2002a), in contrast to values of about 2.5 and 1.2, which would be expected for photolysis; see Kaiser, 2002). This indicates that in the lower stratosphere a much larger fraction than 10% is removed by photo-oxidation (cf. Introduction) and for the samples in the highest bin it might be the primary N_2O sink. This was initially suggested by Röckmann et al. (2001). Note, however, that the error bars are large in spite of the high measurement precision of the present data-set. Especially, the η value has larger analytical errors, even though it should in principle be more sensitive to variations of the $O(^1D)$ contribution to the total N_2O sink, because its end-member values span a larger range than for ψ.

At low N_2O mixing ratios, both η and ψ decline. This is expected from the temper-

ature dependence of η and ψ in N_2O photolysis (Kaiser et al., 2002b) which leads to η and ψ decreases due to the gradual decrease of stratospheric temperatures with altitude. Stratospheric spectral ultraviolet variations are too small to cause effects due to the wavelength dependence of N_2O isotope fractionation (Kaiser et al., 2003b).

Note that the η and ψ values shown here do not correspond to their local values at the point where the sample was obtained, but are convoluted with the η and ψ variations at higher mixing ratios. Nevertheless, any decrease in the local η and ψ values will necessarily also show up in the "globally" calculated values shown here. We tried to derive η and ψ variations from polynomial fits to plots of $\ln(1+{}^2\delta^{15}N)$ vs. $\ln(1+{}^1\delta^{15}N)$ and $\ln(1+\delta^{15}N)$ vs. $\ln(1+\delta^{18}O)$. However, this requires polynomial fits of at least third order, with associated large uncertainties in the regression coefficients. The polynomial fits show negative curvature, i.e., η and ψ decrease with increasing ${}^1\delta^{15}N$ or $\delta^{18}O$ values. However, the uncertainties of the calculated inflection point from this analysis are too high to allow for detecting a change in curvature near the origin.

In conclusion from the position-dependent N_2O isotope measurements, it seems now that they do bear an unambiguous signature of varying contributions of photolysis and photo-oxidation as tentatively established previously (Kaiser, 2002; Röckmann et al., 2001). We also searched for meridional variations in η or ψ by binning the data into polar, mid-latitude and tropical samples. However, no significant meridional contrasts were found and we attribute the suggested lower tropical η values derived from Park et al.'s (2004) re-analysis of our previously published subset of the India 04/99 samples (Röckmann et al., 2001) to analytical artifacts.

4 Conclusions

Apparent fractionation constants (ε_{app}) for stratospheric N_2O are shown to be dependent on the time of sampling (season and year), latitude and altitude. $|\varepsilon_{app}|$ is highest near the equator and decreases towards the poles. Seasonal differences are difficult to discern at polar and tropical latitudes because of limited data coverage, but point

to higher $|\varepsilon_{app}|$ values in fall than in late spring/summer. This can be attributed largely to transport effects (Morgan et al., 2004), with faster transport time scales in the tropics and in fall leading to higher apparent fractionation constants of greater magnitude. Modeling attempts therefore have to consider seasonal and meridional variations of the N_2O isotope signature if quantitative agreement with observations is to be achieved. It might even be necessary to include short-term temporal or longitudinal variations as a comparison between the Gap 06/99 and Sanriku 05/99 profiles shows (Fig. 8 and Sect. 3.2).

In the lower stratosphere (mixing ratios below 200 nmol mol^{-1}), N_2O isotope and mixing ratios display a compact relationship, which can be exploited for calculations of the atmospheric N_2O isotope budget (Kaiser et al., 2004b; Park et al., 2004; Röckmann et al., 2003a). In spite of this compact relationship, lower stratospheric N_2O clearly shows a fingerprint of photo-oxidation in its isotopic signature, as diagnosed from correlations between individual isotope signatures. Stronger variations in the correlation between $\delta^{15}N$, $\delta^{18}O$ and the position-dependent $\delta^{15}N$ values can be unambiguously detected in the upper stratosphere. These might be explained by temperature effects (Kaiser, 2002; Kaiser et al., 2002b).

We have also discussed conceptual models to rationalize stratospheric N_2O isotope variations in the framework of modified Rayleigh fractionation (considering a one-dimensional reaction-diffusion-advection scheme), end-member mixing and continuous weak mixing between intravortex and extravortex air (Plumb et al., 2000). None of the models captures all stratospheric features. Especially, aircraft samples from the polar vortex at N_2O mixing ratios below 200 nmol mol^{-1} deviate both from isotope variations expected for Rayleigh fractionation and end-member mixing, but could be explained by continuous weak mixing between extravortex and intravortex air. More detailed three-dimensional model simulations will be needed to fully appraise the expanding set of stratospheric N_2O isotope measurements.

Acknowledgements. We would like to thank B. Knape for help with the mass-spectrometric measurements and A. Plumb for useful discussions about a conceptual model of continuous

weak mixing. Thanks to M. Braß for providing CH_4 mixing ratios and to D. Griffith for useful discussions on slopes in Rayleigh fractionation plots. The ISOSTRAT project in Heidelberg was funded by the BMBF within the AFO2000 project (grant 07ATC01). We thank CNES for excellent performance of the mid- and high-latitude balloon launches. Funding from various projects of ESA, DLR, BMBF and the European Commission is gratefully acknowledged for the balloon operations.

References

Bender, M. L.: The $\delta^{18}O$ of dissolved O_2 in seawater: A unique tracer of circulation and respiration in the deep sea, J. Geophys. Res., 95, 22 243–22 252, 1990.

Bernard, S., Röckmann, T., Kaiser, J., Barnola, J.-M., Fischer, H., Blunier, T., and Chappellaz, J.: Constraints on N_2O budget changes since pre-industrial time from new firn air and ice core isotope measurements, Atmos. Chem. Phys., 6, 493–503, 2006.

Boering, K. R., Wofsy, S. C., Daube, B. C., Schneider, H. R., Loewenstein, M., Podolske, J. R., and Conway, T. J.: Stratospheric mean ages and transport rates from observations of carbon dioxide and nitrous oxide, Science, 274, 1340–1343, 1996.

Brenninkmeijer, C. A. M. and Röckmann, T.: Mass spectrometry of the intramolecular nitrogen isotope distribution of environmental nitrous oxide using fragment-ion analysis, Rapid Commun. Mass Spectrom., 13, 2028–2033, 1999.

Engel, A., Strunk, M., Müller, M., Haase, H.-P., Poss, C., Levin, I., and Schmidt, U.: Temporal development of total chlorine in the high-latitude stratosphere based on reference distributions of mean age derived from CO_2 and SF_6, J. Geophys. Res., 107, 1–11, 2002.

Engel, A., Möbius, T., Haase, H.-P., Bönisch, H., Wetter, T., Schmidt, U., Levin, I., Reddmann, T., Oelhaf, H., Grunow, K., Huret, N., and Pirre, M.: Observation of mesospheric air inside the arctic stratospheric polar vortex in early 2003, Atmos. Chem. Phys., 6, 267–282, 2006.

Esler, M. B., Griffith, D. W. T., Wilson, S. R., and Steele, L. P.: Precision trace gas analysis by FT-IR spectroscopy. 1. Simultaneous analysis of CO_2, CH_4, N_2O, and CO in air, Anal. Chem., 72, 206–215, 2000.

Griffith, D. W. T., Toon, G. C., Sen, B., Blavier, J.-F., and Toth, R. A.: Vertical profiles of nitrous oxide isotopomer fractionation measured in the stratosphere, Geophys. Res. Lett., 27, 2485–2488, 2000.

Johnston, J. C., Cliff, S. S., and Thiemens, M. H.: Measurement of multioxygen isotopic ($\delta^{18}O$ and $\delta^{17}O$) fractionation factors in the stratospheric sink reactions of nitrous oxide, J. Geophys. Res., 100, 16 801–16 804, 1995.

Kaiser, J.: Stable isotope investigations of atmospheric nitrous oxide (http://archimed.uni-mainz.de/pub/2003/0004/), Ph.D. thesis, Johannes Gutenberg-Universität, Mainz, 2002.

Kaiser, J., Brenninkmeijer, C. A. M., and Röckmann, T.: Intramolecular ^{15}N and ^{18}O fractionation in the reaction of N_2O with $O(^1D)$ and its implications for the stratospheric N_2O isotope signature, J. Geophys. Res., 107, 4214, doi:10.1029/2001JD001506, 2002a.

Kaiser, J., Röckmann, T., and Brenninkmeijer, C. A. M.: Temperature dependence of isotope fractionation in N_2O photolysis, Phys. Chem. Chem. Phys., 4, 4220–4230, doi:10.1039/B204837J, 2002b.

Kaiser, J., Röckmann, T., and Brenninkmeijer, C. A. M.: Complete and accurate mass-spectrometric isotope analysis of tropospheric nitrous oxide, J. Geophys. Res., 108, 4476, doi:10.1029/2003JD003613, 2003a.

Kaiser, J., Röckmann, T., Brenninkmeijer, C. A. M., and Crutzen, P. J.: Wavelength dependence of isotope fractionation in N_2O photolysis, Atmos. Chem. Phys., 3, 303–313, 2003b.

Kaiser, J., Park, S., Boering, K. A., Brenninkmeijer, C. A. M., Hilkert, A. W., and Röckmann, T.: Mass-spectrometric method for the absolute calibration of the intramolecular nitrogen isotope distribution in nitrous oxide, Anal. Bioanal. Chem., 378, 256–269, doi:10.1007/s00216-003-2233-2, 2004a.

Kaiser, J., Röckmann, T., and Brenninkmeijer, C. A. M.: Contribution of mass-dependent fractionation to the oxygen isotope anomaly of atmospheric nitrous oxide, J. Geophys. Res., 109, D03305, doi:10.1029/2003JD004088, 2004b.

Kaiser, J. and Röckmann, T.: Absence of isotope exchange in the reaction of N_2O + $O(^1D)$ and the global $\Delta^{17}O$ budget of nitrous oxide, Geophys. Res. Lett., 32, L15808, doi:10.1029/2005GL023199, 2005.

Kaye, J. A.: Mechanisms and observations for isotope fractionation of molecular species in planetary atmospheres, Rev. Geophys., 25, 1609–1658, 1987.

Kim, K.-R. and Craig, H.: Nitrogen-15 and oxygen-18 characteristics of nitrous oxide: A global perspective, Science, 262, 1855–1857, 1993.

McLinden, C. A., Prather, M. J., and Johnson, M. S.: Global modeling of the isotopic analogues

of N_2O: Stratospheric distributions, budgets, and the ^{17}O-^{18}O mass-independent anomaly, J. Geophys. Res., 108, 4233, doi:10.1029/2002JD002560, 2003.
Michelsen, H. A., Manney, G. L., Gunson, M. R., Rinsland, C. P., and Zander, R.: Correlations of stratospheric abundances of CH_4 and N_2O derived from ATMOS measurements, Geophys. Res. Lett., 25, 2777–2780, 1998.
Minschwaner, K., Salawitch, R. J., and McElroy, M. B.: Absorption of solar radiation by O_2: Implications for O_3 and lifetimes of N_2O, $CFCl_3$, and CF_2Cl_2, J. Geophys. Res., 98, 10 543–10 561, 1993.
Moore, H.: Isotopic measurement of atmospheric nitrogen compounds, Tellus, 26, 169–174, 1974.
Morgan, C. G., Allen, M., Liang, M. C., Shia, R. L., Blake, G. A., and Yung, Y. L.: Isotopic fractionation of nitrous oxide in the stratosphere: Comparison between model and observations, J. Geophys. Res., 109, D04305, doi:10.1029/2003JD003402, 2004.
Park, S., Atlas, E. L., and Boering, K. A.: Measurements of N_2O isotopologues in the stratosphere: Influence of transport on the apparent enrichment factors and the isotope fluxes to the troposphere, J. Geophys. Res., 109, D01305, doi:10.1029/2003JD003731, 2004.
Patra, P. K., Lal, S., Venkataramani, S., and Chand, D.: Halogen Occultation Experiment (HALOE) and balloon-borne in situ measurements of methane in stratosphere and their relation to the quasi-biennial oscillation (QBO), Atmos. Chem. Phys., 3, 1051–1062, 2003.
Plumb, R. A., Waugh, D. W., and Chipperfield, M. P.: The effects of mixing on tracer relationships in the polar vortices, J. Geophys. Res., 105, 10 047–10 062, 2000.
Prather, M., Ehhalt, D., Dentener, F., Derwent, R., Dlugokencky, E., Holland, E., Isaksen, I., Katima, J., Kirchhoff, V., Matson, P., Midgley, P., and Wang, M.: Atmospheric chemistry and greenhouse gases, in: Climate Change 2001: The Scientific Basis, edited by: Houghton, J. T., Ding, Y., Griggs, D. J., et al., 239–287, Cambridge University Press, 2001.
Prinn, R. G., Weiss, R. F., Fraser, P. J., Simmonds, P. G., Cunnold, D. M., Alyea, F. N., O'Doherty, S., Salameh, P., Miller, B. R., Huang, J., Wang, R. H. J., Hartley, D. E., Harth, C., Steele, L. P., Sturrock, G., Midgley, P. M., and McCulloch, A.: A history of chemically and radiatively important gases in air deduced from ALE/GAGE/AGAGE, J. Geophys. Res., 105, 17 751–17 792, 2000.
Rahn, T. and Wahlen, M.: Stable isotope enrichment in stratospheric nitrous oxide, Science, 278, 1776–1778, 1997.
Rahn, T., Zhang, H., Wahlen, M., and Blake, G. A.: Stable isotope fractionation during ultraviolet

photolysis of N_2O, Geophys. Res. Lett., 25, 4489–4492, 1998.
Röckmann, T., Kaiser, J., Brenninkmeijer, C. A. M., Crowley, J. N., Borchers, R., Brand, W. A., and Crutzen, P. J.: The isotopic enrichment of nitrous oxide ($^{15}N^{14}NO$, $^{14}N^{15}NO$, $^{14}N^{14}N^{18}O$) in the stratosphere and in the laboratory, J. Geophys. Res., 106, 10 403–10 410, 2001.
Röckmann, T., Kaiser, J., and Brenninkmeijer, C. A. M.: The isotopic fingerprint of the pre-industrial and the anthropogenic N_2O source, Atmos. Chem. Phys., 3, 315–323, 2003a.
Röckmann, T., Kaiser, J., Brenninkmeijer, C. A. M., and Brand, W. A.: Gas-chromatography/isotope-ratio mass spectrometry method for high-precision position-dependent ^{15}N and ^{18}O measurements of atmospheric nitrous oxide, Rapid Commun. Mass Spectrom., 17, 1897–1908, 2003b.
Röckmann, T. and Levin, I.: High-precision determination of the changing isotopic composition of atmospheric N_2O from 1990 to 2002, J. Geophys. Res., 110, D21304, doi:10.1029/2005JD006066, 2005.
Schmidt, U., Kulessa, G., Klein, E., Roth, E. P., Fabian, P., and Borchers, R.: Intercomparison of balloon-borne cryogenic whole air samplers during the MAP/GLOBUS 1983 campaign, Planet. Space Sci., 35, 647, 1987.
Selwyn, G. S. and Johnston, H. S.: Ultraviolet absorption spectrum of nitrous oxide as function of temperature and isotopic substitution, J. Chem. Phys., 74, 3791–3803, 1981.
Sowers, T., Rodebaugh, A., Yoshida, N., and Toyoda, S.: Extending records of the isotopic composition of atmospheric N_2O back to 1800 A.D. from air trapped in snow at the South Pole and the Greenland Ice Sheet Project II ice core, Global Biogeochem. Cycles, 16, 1129, doi:10.1029/2001GB001911, 2002.
Toyoda, S. and Yoshida, N.: Determination of nitrogen isotopomers of nitrous oxide on a modified isotope ratio mass spectrometer, Anal. Chem., 71, 4711–4718, 1999.
Toyoda, S., Yoshida, N., Urabe, T., Aoki, S., Nakazawa, T., Sugawara, S., and Honda, H.: Fractionation of N_2O isotopomers in the stratosphere, J. Geophys. Res., 106, 7515–7522, 2001.
Toyoda, S., Yoshida, N., Urabe, T., Nakayama, Y., Suzuki, T., Tsuji, K., Shibuya, K., Aoki, S., Nakazawa, T., Ishidoya, S., Ishijima, K., Sugawara, S., Machida, T., Hashida, G., Morimoto, S., and Honda, H.: Temporal and latitudinal distributions of stratospheric N_2O isotopomers, J. Geophys. Res., 109, D08308, doi:10.1029/2003JD004316, 2004.
Volk, C. M., Elkins, J. W., Fahey, D. W., Dutton, G. S., Gilligan, J. M., Loewenstein, M., Podolske, J. R., Chan, K. R., and Gunson, M. R.: Evaluation of source gas lifetimes from stratospheric

observations, J. Geophys. Res., 102, 25 543–25 563, 1997.
von Hessberg, P., Kaiser, J., Enghoff, M. B., McLinden, C. A., Sorensen, S. S., Röckmann, T., and Johnson, M. S.: Ultra-violet absorption cross sections of isotopically substituted nitrous oxide species: $^{14}N^{14}NO$, $^{15}N^{14}NO$, $^{14}N^{15}NO$ and $^{15}N^{15}NO$, Atmos. Chem. Phys., 4, 1237–1253, 2004.
Yoshida, N., Morimoto, H., and Matsuo, S.: UV photolysis and microbial reduction as major sinks of nitrous oxide with emphasis on kinetic nitrogen isotope discrimination, Eos Trans. AGU, 71, 933–934, 1990.
Yoshida, N. and Toyoda, S.: Constraining the atmospheric N_2O budget from intramolecular site preference in N_2O isotopomers, Nature, 405, 330–334, 2000.
Yung, Y. L. and Miller, C. E.: Isotopic fractionation of stratospheric nitrous oxide, Science, 278, 1778–1780, 1997.

Table 1. Sampling dates and locations of past upper tropospheric and stratospheric N_2O isotope measurements. Unknown dates are marked by x's. Most isotope measurements have been performed by isotope-ratio mass spectrometry (IRMS), except for the Fourier transform infrared spectroscopic (FTIR) data of Griffith et al. (2000).

Location or campaign	Date	Latitude °N	Longitude °E	Altitude km	Samples	Reference
Mildura, Australia	xx xxx 197x	−34	142	21	1	Moore (1974)
Kiruna, Sweden	10 Jan 1988	68	20	13	1	Kim and Craig (1993)
	10 Feb 1988	68	20	18	1	
Kiruna, Sweden	10 Feb 1988	68	20	14+23	2	Rahn and Wahlen (1997)
Contiguous USA	27 Jan 1988	46	−94	17	1	
	10 May 88	39–45	−94	17+18	2	
	12 April 1989	40–48	−94	15+17	2	
Fort Sumner, USA	14 Sep 1992	34	−104	18–35	1 profile	Griffith et al. (2000)
	15 Sep 1992	34	−104	18–35	1 profile	
	25 Sep 1993	34	−104	18–35	1 profile	
	26 Sep 1993	34	−104	18–35	1 profile	
	22 May 1994	34	−104	18–35	1 profile	
	28 Sep 96	34	−104	18–35	1 profile	
Fairbanks, USA	8 May 1997	65	−148	18–32	1 profile	
	7 July 1997	65	−148	18–30	1 profile	
Kiruna, Sweden	3 Dec 1999	68	1	18–32	1 profile	
POLARIS I	26 April 1997	81–88	n/a	17–19	4	Park et al. (2004)
POLARIS II	29 June 1997	62	n/a	21	1	
	30 June 1997	63–66	n/a	19–21	3	
	7 July 1997	73–89	n/a	17–21	3	
	10 July 1997	64	n/a	21	1	
POLARIS III	15 Sep 1997	65	n/a	13–19	4	
	18 Sep 1997	79	n/a	19	1	
SOLVE	23 Jan 2000	63–65	n/a	11–18	3	
	27 Jan 2000	63–66	n/a	20	3	
	2 Feb 2000	64	n/a	19	1	
	3 Feb 2000	69	n/a	18	1	
	5 March 2000	68–70	n/a	17–19	2	
	11 March 2000	61–72	n/a	17–20	5	

Table 1. Continued.

Location or campaign	Date	Latitude °N	Longitude °E	Altitude km	Samples	Reference
Sanriku, Japan	4 June 1990	39	142	16–35	9	Toyoda et al. (2001, 2004),
	3 Sep 1998	39	142	15–30	11	Yoshida and Toyoda (2000)
	31 May 1999	39	142	15–35	11	
	28 Aug 2000	39	142	15–32	10	
	30 May 2001	39	142	15–34	11	
Kiruna, Sweden	22 Feb 1997	68	20	10–26	11	
Syowa, Antarctica	3 Jan 1998	−69	40	10–30	9	
Hyderabad, India	26 March 1987	18	79	17–26	5	Röckmann et al. (2001; this work)
	29 April 1999	18	79	10–28	10	
Aire sur l'Adour	30 Sep 1993	44	0	10–32	14	
(ASA), France	9 Oct 2001	44	−1	12–31	14	
	24 Sep 2002	44	0–1	12–32	9	
Gap, France	23 June 1999	44	3–6	8–34	15	
Kiruna, Sweden	18 Jan 1992	68	21	6–27	2	
	6 Feb 1992	68	21	7–23	9	
	20 March 1992	68	21	7–25	9	
	7 March 1995	68	21	7–30	11	
	1 March 2000	68	24–28	9–21	11	
	6 March 2003	68	22–27	11–30	13	
EUPLEX	19 Jan 2003	77	21	20	1	
	23 Jan 2003	66–73	16–18	18–20	13	
	26 Jan 2003	66–73	21–23	18–19	5	
	6 Feb 2003	66–79	9–19	17–20	16	
	8 Feb 2003	67–72	15–27	17–20	18	
	9 Feb 2003	68–80	23–49	14–19	19	
	11 Feb 2003	67–70	12–26	8–15	16	

Table 2. Apparent Rayleigh fractionation constants (ε_{app}) derived for lower stratospheric samples (linear fit for $\ln(\mu/\mu_T)>-0.6$) and for middle stratospheric samples at $\ln(\mu/\mu_T)$ values of −1.0, −1.5 and −2.0 (first derivative of second order polynomial fit for $\ln(\mu/\mu_T)>-2.4$). Extrapolated values are shown in parentheses.

	$-\varepsilon^{15}N_{app}$				$-\varepsilon^{18}O_{app}$			
$\ln(\mu/\mu_T)$	>−0.6	−1.0	−1.5	−2.0	> −0.6	−1.0	−1.5	−2.0
India 03/87	19±1				16±1			
India 04/99	18±1	(27±1)			16±1	(22±2)		
ASA 09/93	17±0	23±1	30±1	(36±1)	14±0	19±1	25±1	(31±1)
ASA 10/01	19±1	25±2	(30±3)		15±1	20±2	(25±2)	
ASA 09/02	16±0	24±4	(30±4)		12±0	19±4	(24±4)	
Gap 06/99	17±1	21±1	24±1	27±1	14±1	17±1	20±1	22±1
Kiruna 01/92	17±0	20±0	23±1	25±1	14±0	17±1	19±1	21±1
Kiruna 02/92	14±0	21±3	25±3	28±4	13±1	18±1	21±1	24±2
Kiruna 03/92	17±1	17±0	18±1	20±1	16±1	14±1	16±1	17±2
Kiruna 03/95	17±1	21±2	23±3	(26±3)	13±1	17±2	20±2	(22±2)
Kiruna 03/00	15±1	19±1	22±1	25±1	13±1	16±1	18±1	21±1
Kiruna 03/03	14±0	17±0	19±0	21±0	9±1	13±1	15±1	18±1
EUPLEX 02/03	15±0	18±0	(20±0)		12±0	14±0	(16±0)	
	$-^2\varepsilon^{15}N_{app}$				$-^1\varepsilon^{15}N_{app}$			
$\ln(\mu/\mu_T)$	>−0.6	−1.0	−1.5	−2.0	>−0.6	−1.0	−1.5	−2.0
India 03/87	27±2				11±1			
India 04/99	25±2	(37±3)			10±1	(16±3)		
ASA 09/93	23±1	33±2	42±2	(51±2)	10±1	13±1	16±1	(20±1)
ASA 10/01	27±1	37±4	(46±5)		9±1	12±3	(12±3)	
ASA 10/02	22±1	33±9	(40±12)		9±1	16±3	(23±4)	
Gap 06/99	25±1	31±1	34±2	38±2	9±1	10±1	12±2	14±2
Kiruna 01/92	23±1	28±1	32±1	35±1	11±0	12±0	13±0	15±1
Kiruna 02/92	23±1	31±2	35±2	39±3	5±0	12±3	14±4	17±5
Kiruna 03/92	22±2	26±1	27±1	28±1	11±3	8±2	10±2	11±2
Kiruna 03/95	25±2	30±3	34±4	(37±4)	8±1	10±2	12±2	(14±2)
Kiruna 01/00	22±2	29±0	32±0	36±0	4±1	9±0	12±0	14±0
Kiruna 03/03	19±2	24±2	27±2	29±2	8±3	9±2	10±2	12±2
EUPLEX 02/03	22±0	26±1	(29±1)		9±0	10±1	(11±1)	

ACPD
6, 4273–4324, 2006

EGU

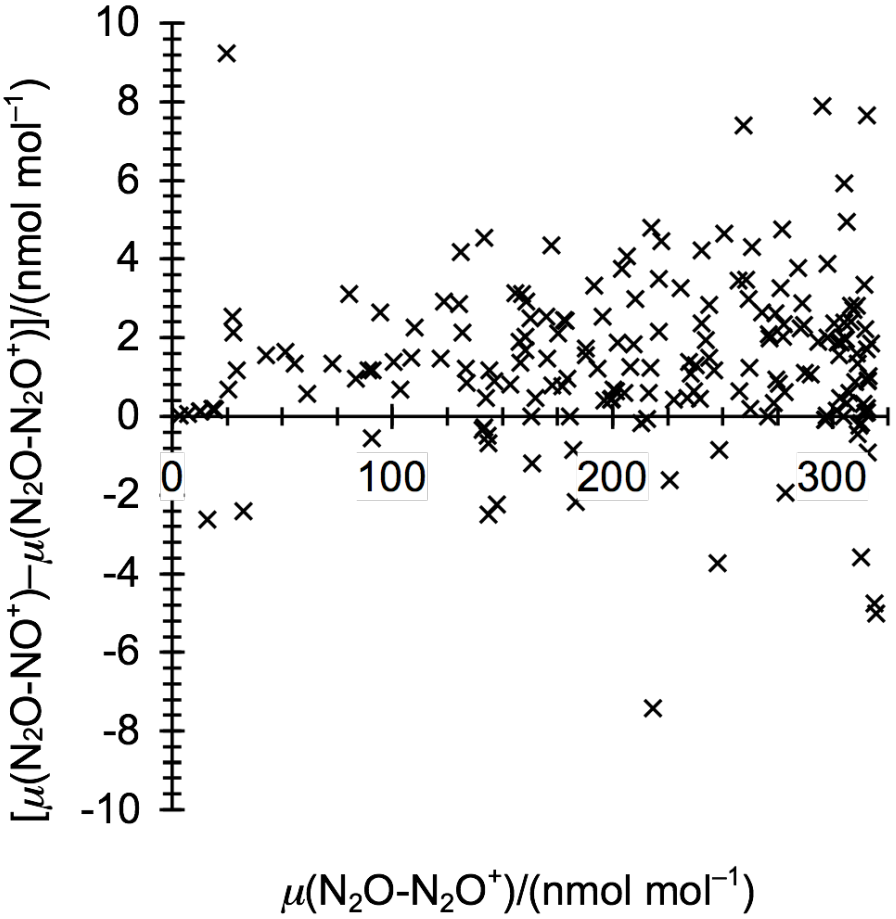

Fig. 1. Difference between N_2O mixing ratios derived from the NO^+ fragment ion and the N_2O^+ molecular ion peak areas versus N_2O mixing ratios derived from the N_2O^+ molecular ion peak area (195 of 213 samples). The average difference is (1.3±2.1) nmol mol^{-1}.

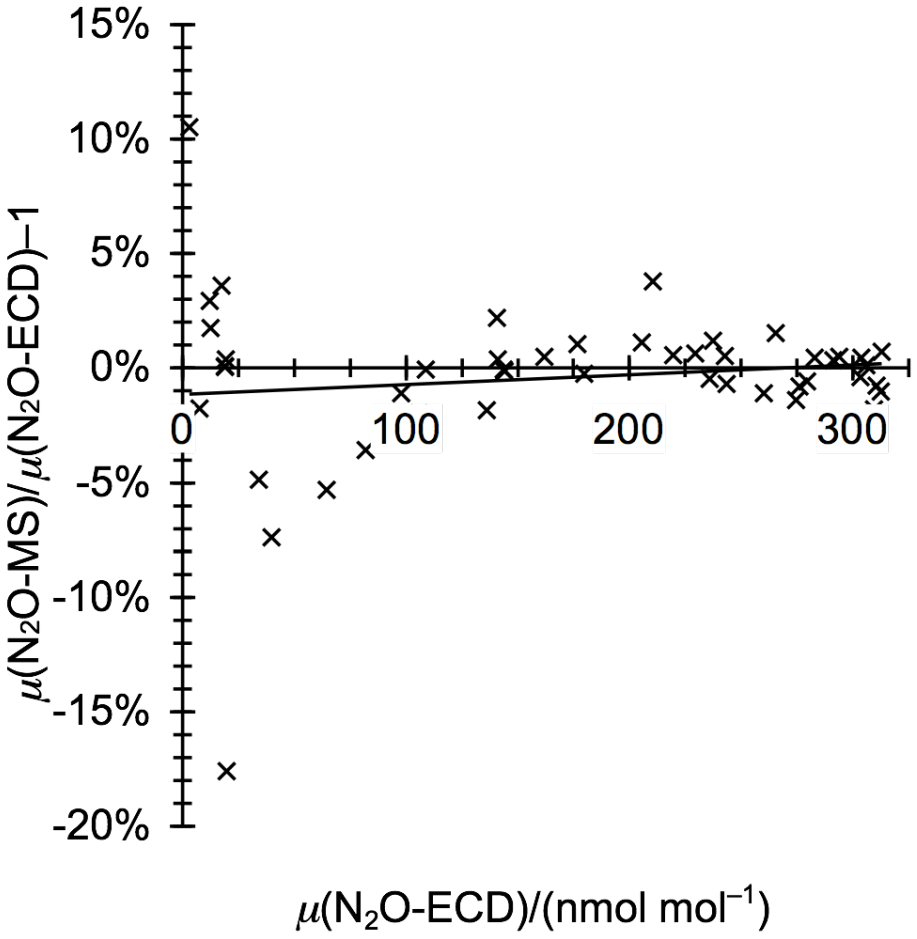

Fig. 2. Relative difference between N_2O mixing ratio determined with mass-spectrometric (MS) and electron capture detection (ECD) versus N_2O mixing ratio determined by ECD (47 of 213 samples). The average relative difference is (−0.3±2.1)%, excluding two outliers of 11% and −18%.

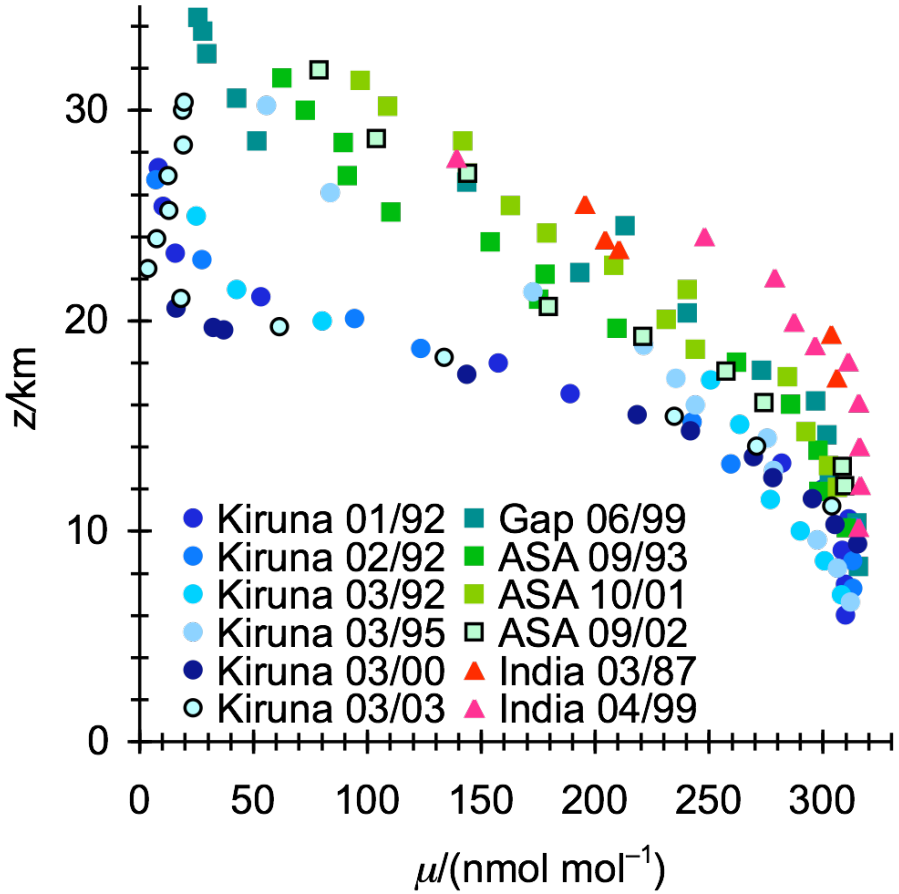

Fig. 3. Vertical profiles of N_2O mixing ratios from the balloon flights (ASA: Aire sur l'Adour). The EUPLEX 2003 aircraft samples have been omitted to avoid congestion of the plot. The mixing ratios have not been adjusted for the sampling date and the stratospheric age of air (Sect. 3.2).

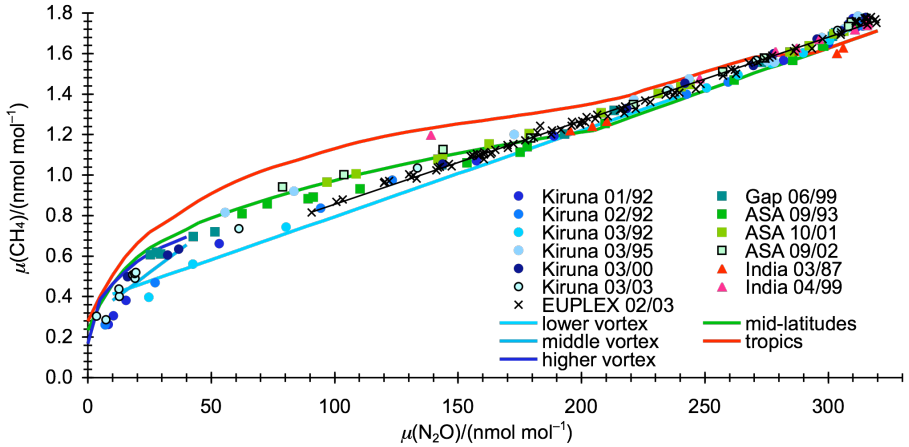

Fig. 4. Correlation between CH_4 and N_2O mixing ratios, measured by gas chromatography-isotope ratio mass spectrometry. Reference curves for vortex, mid-latitude and tropical air are from ATMOS measurements (Michelsen et al., 1998).

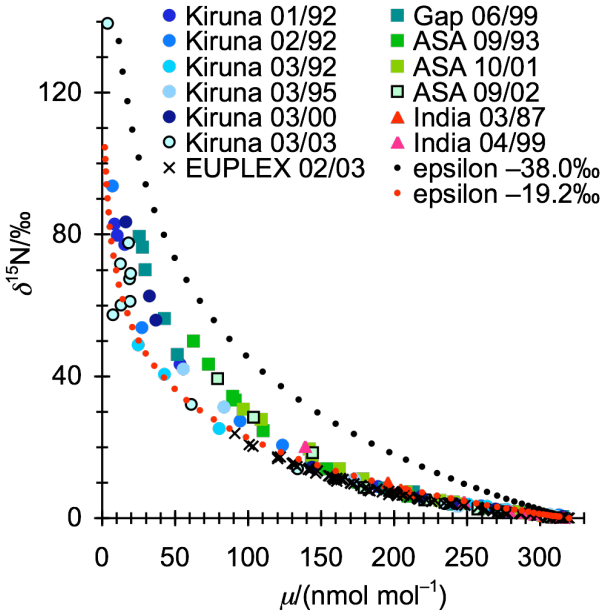

Fig. 5. Compact relationship between δ values and mixing ratios down to 200 nmol mol^{-1}, divergent relationship below, with higher δ values for mid-latitude samples than for polar locations. However, note the mid-latitude profile for Kiruna 03/95 (outside of polar vortex), which was classified as a mid-latitude profile based on its CH_4-N_2O correlation (Sect. 3.2 and Fig. 4), but is within the range of other polar profiles in δ-μ space. δ values are relative to SIL-N_2O. Also shown are two hypothetical Rayleigh fractionation lines, which have been calculated assuming isotope effects ε of –38.0‰ and –19.2‰, respectively. These two limits for ε correspond to an intrinsic photochemical isotope effect as expected from broadband photolysis at room temperature with a 10% contribution from N_2O photo-oxidation and the apparent isotope effect expected for transport-limited conditions (about half the intrinsic isotopic effect) (Kaiser et al., 2002a, b).

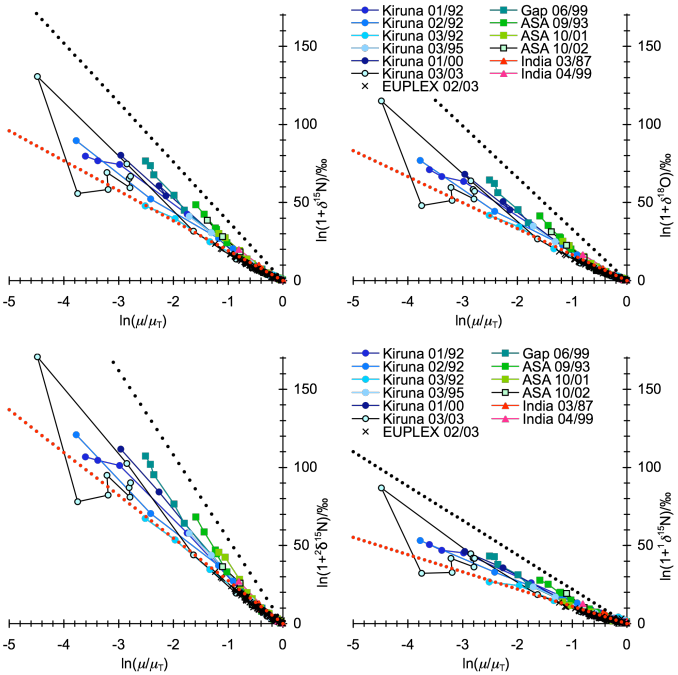

Fig. 6. Rayleigh plots for bulk nitrogen, oxygen and position-dependent nitrogen isotope signatures of stratospheric N_2O. The δ values are expressed relative to the isotopic composition of tropopause N_2O at the time the sample entered the stratosphere, which takes the decreasing heavy isotope content of tropospheric N_2O and the age of the stratospheric air sample into account. Similarly, the mixing ratio of tropopause N_2O that we use to calculate $\ln(\mu/\mu_T)$ is corrected for the increasing atmospheric N_2O mixing ratio and the age of air (see Sect. 3.2 for details). Black and red dotted lines correspond to Rayleigh fractionation with fractionation constants $\varepsilon^{15}N=-38.0‰/-19.2‰$, $\varepsilon^{18}O=-33‰/-16.6‰$, $^1\varepsilon^{15}N=-22.0/-11.1‰$, and $^2\varepsilon^{15}N=-54.0‰/-27.4‰$, respectively.

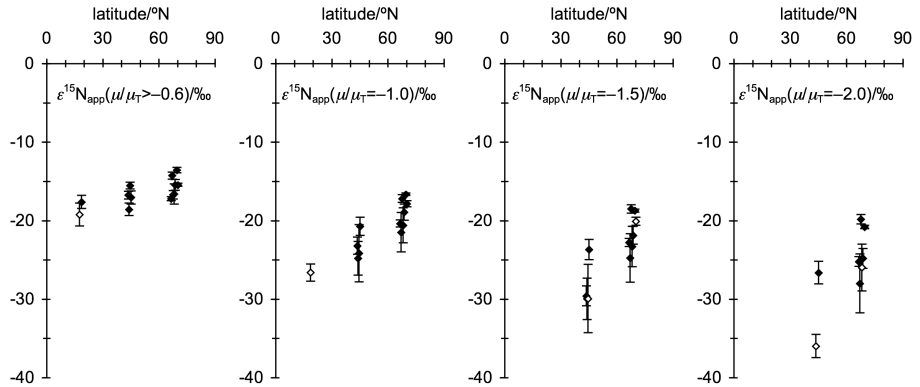

Fig. 7. Dependence of the apparent Rayleigh fractionation constant, $\varepsilon^{15}N_{app}$, on latitude and remaining N_2O fraction (μ/μ_T). For better visibility, data points at the same latitude have been separated by 0.5° in the plot. Extrapolated values are shown as open symbols. The apparent fractionation constants have been derived from a linear fit to the data points with $\mu/\mu_T>-0.6$ and from the local slope of second-order polynomial fits at $\mu/\mu_T=-1.0$, -1.5, and -2.0.

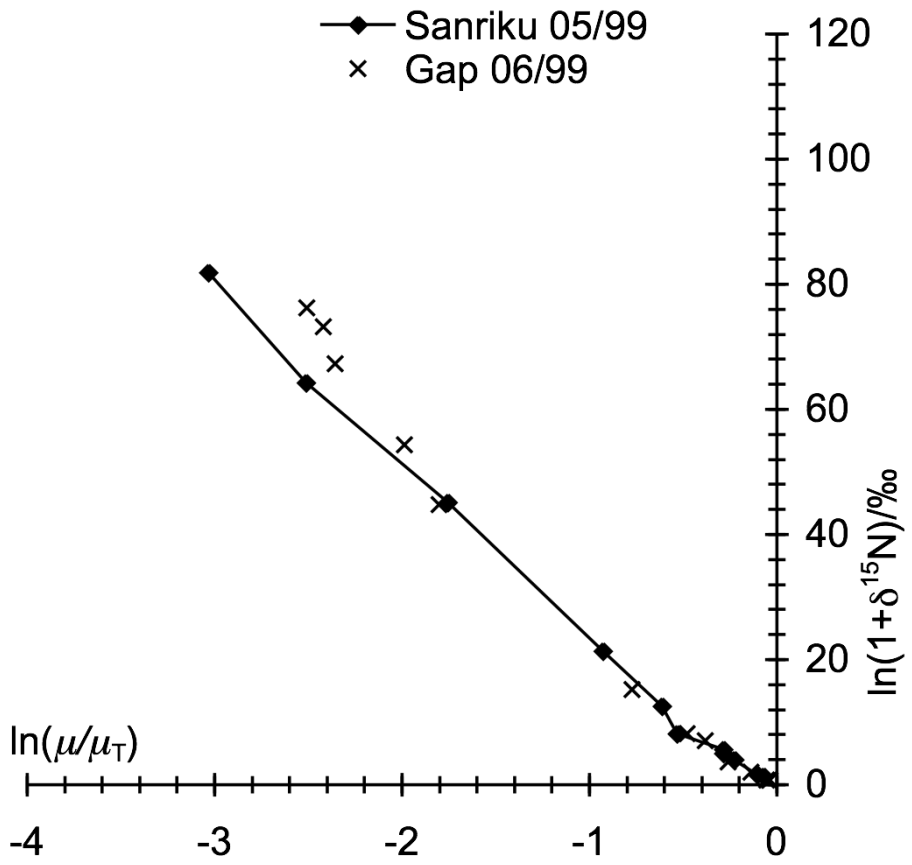

Fig. 8. Comparison between two stratospheric N_2O profiles obtained at nearly the same time and same latitude, but at different longitudes (Gap 23 June 1999: 3–6° E, Sanriku 31 May 1999: 142° E). The mixing ratios and δ values have been normalized to the same stratospheric entrance date.

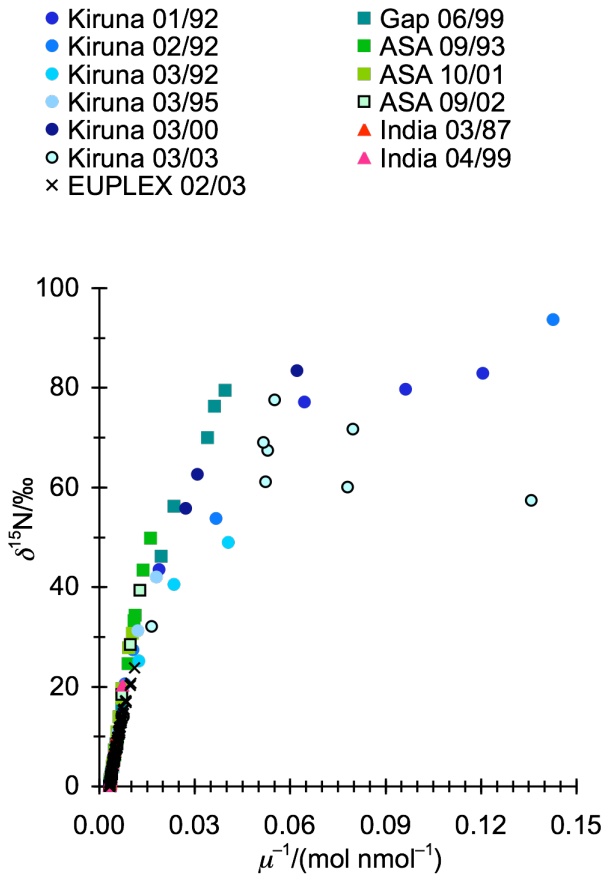

Fig. 9. Mixing plot of the bulk nitrogen isotope ratio. End-member mixing would lead to a linear relationship in a $\delta - \mu^{-1}$ plot. One Kiruna 03/03 sample at 0.283 mol nmol^{-1}/139.6‰ (3.5 nmol mol^{-1}) has been omitted in order to show details for samples with higher mixing ratios more clearly.

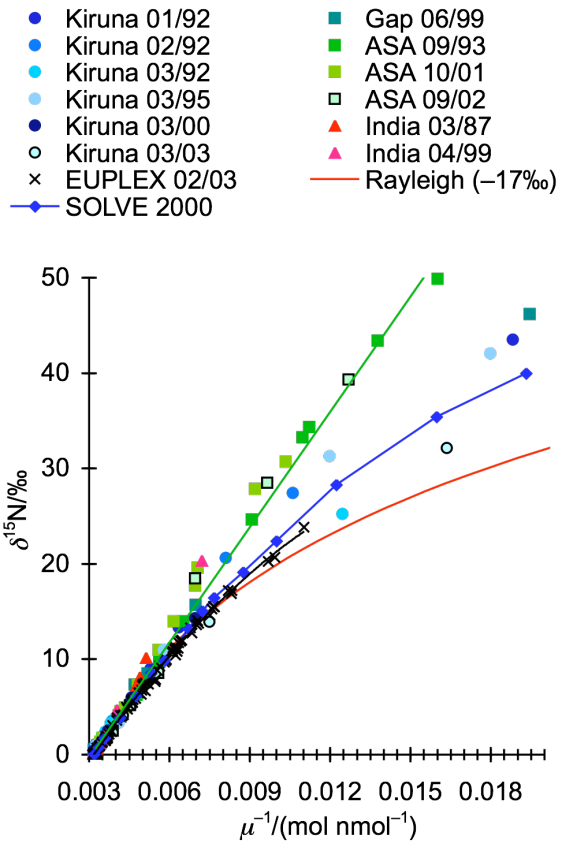

Fig. 10. Linear end-member mixing for some mid-latitude samples, e.g. δ^{15}N(ASA 09/93)=4.0·10^{-9} μ^{-1}−12.4‰ (R^2=0.997); weak mixing (?) at polar latitudes, δ^{15}N(EUPLEX 2003)=−1.4·10^{-16} μ^{-2}+4.9·10^{-9} μ^{-1}−14.2‰ (R^2=0.998). Also shown is a Rayleigh-fractionation curve with a fractionation constant of ε=−17‰.

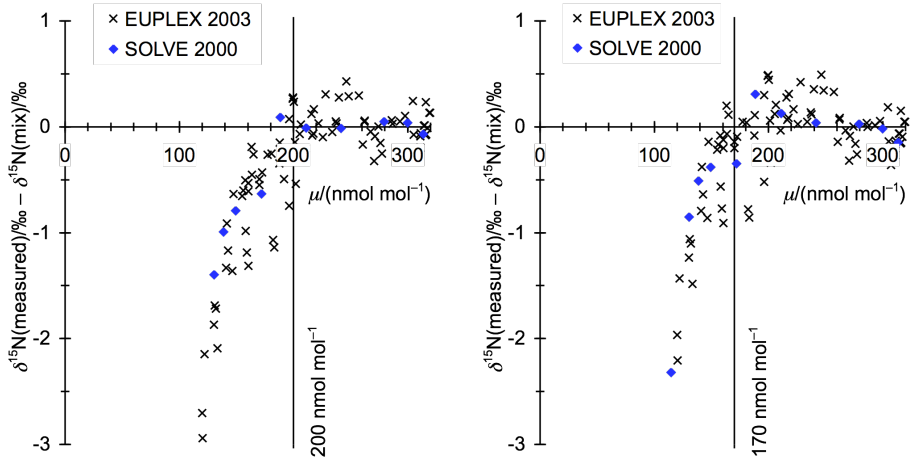

Fig. 11. Residuals of linear fits to polar aircraft N_2O measurements. No structure is visible in the residuals for a lower cut-off of 200 nmol mol^{-1} (left panel), but if a lower cut-off of 170 nmol mol^{-1} (right panel) is used for the linear fits, samples closer to 170 nmol mol^{-1} fall mostly above the x-axis, while samples closer to 300 nmol mol^{-1} fall mostly below the x-axis.

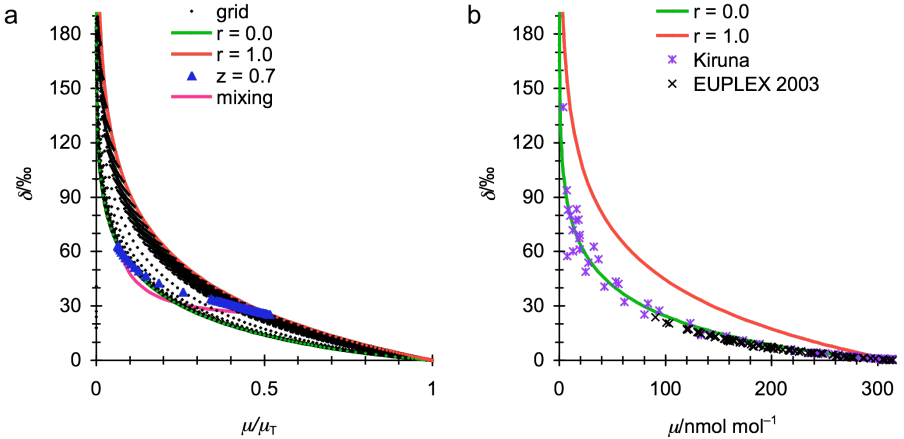

Fig. 12. (a) Plot of δ value vs. normalized mixing ratio for a continuous weak mixing model on a 41×101 (r×z) grid (based on Plumb et al., 2000). Grid boundaries at r=0.0 and r=1.0, a horizontal cross-section at z=0.7 as well as a hypothetical mixing curve between the (0.0, 0.7) and (1.0, 0.7) end-members are indicated. Continuous weak mixing leads to a clustering of the δ values near the curves defined by the grid boundaries. These correspond to the intravortex (polar) and extravortex (midlatitude) regions. The values the r=1.0 grid boundary corresponds to the assumed constant isotope effect of ε=−38‰. **(b)** Comparison between polar stratospheric measurements from balloon and aircraft campaigns at Kiruna with continuous weak mixing model results at the grid boundaries. The normalized mixing ratios from the model runs have been multiplied by an N_2O mixing ratio of 314 nmol mol^{-1} (1998) to facilitate the comparison to stratospheric measurements.

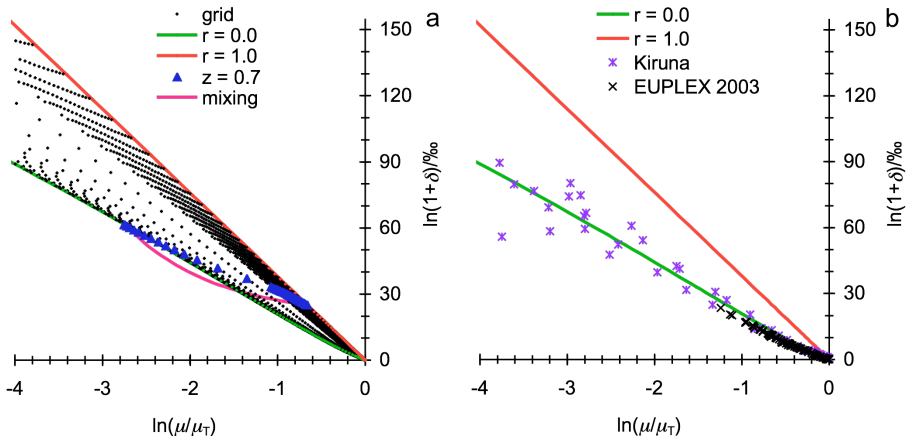

Fig. 13. Same as Fig. 12, but now plotted as $\ln(1+\delta)$ vs. $\ln(\mu/\mu_T)$.

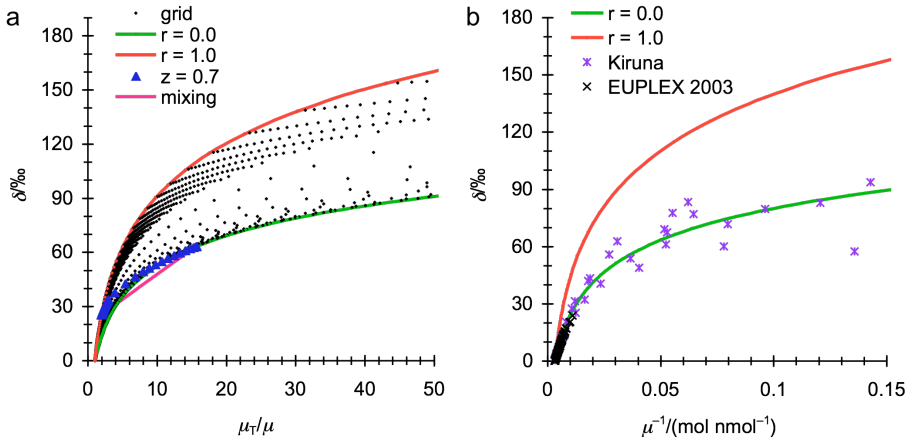

Fig. 14. Same as Fig. 12, but now plotted as δ value vs. normalized inverse mixing ratio, μ_T/μ, or inverse mixing ratio, μ^{-1}.

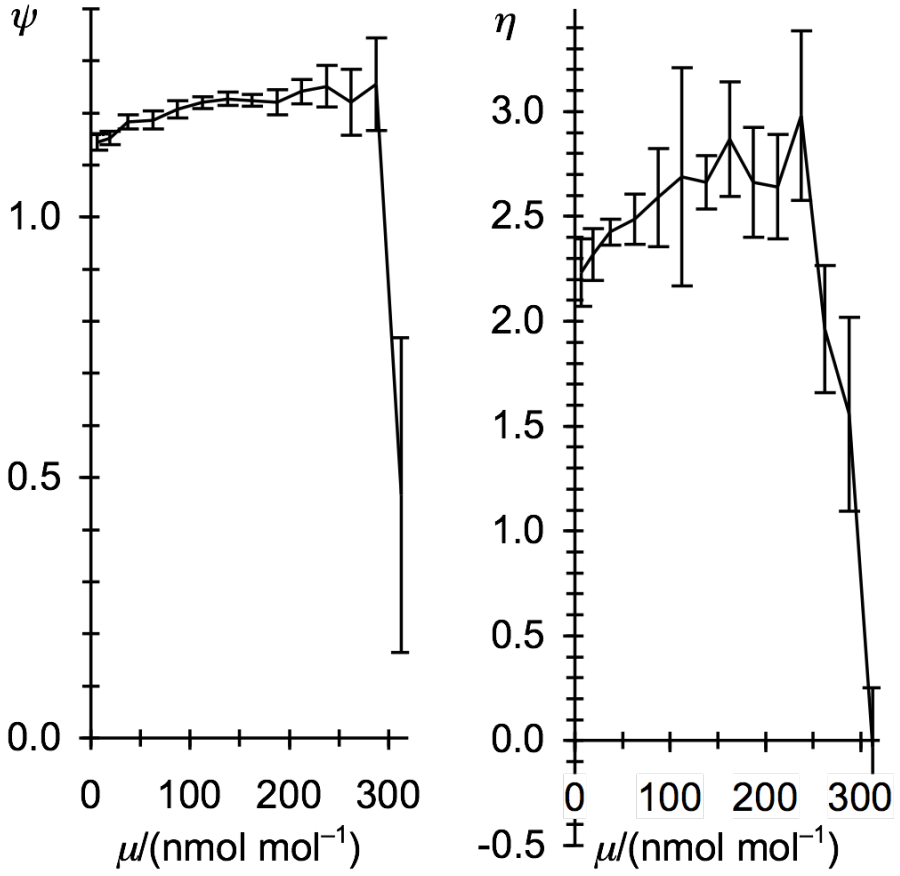

Fig. 15. Dependence of binned ψ- and η-values on the N_2O mixing ratio. Error bars correspond to the standard error of the mean for the respective mixing ratio bin.

ACPD
6, 4273–4324, 2006

EGU